Environmental Science: Atmospheres

ROYAL SOCIETY OF CHEMISTRY

PAPER

View Article Online
View Journal | View Issue

Cite this: *Environ. Sci.: Atmos.*, 2022, **2**, 659

O_3–NO_y photochemistry in boundary layer polluted plumes: insights from the MEGAPOLI (Paris), ChArMEx/SAFMED (North West Mediterranean) and DACCIWA (southern West Africa) aircraft campaigns†

B. Thera,[a] P. Dominutti,[ab] A. Colomb,[a] V. Michoud,[c] J.-F. Doussin,[d] M. Beekmann,[c] F. Dulac,[e] K. Sartelet[f] and A. Borbon *[a]

The ozone–NO_y photochemistry is explored in contrasting polluted plumes sampled with the Safire ATR 42 research aircraft during three summer field international campaigns in the megacity Paris, the North West Mediterranean basin (WMB) and southern West Africa (SWA). Various metrics derived from the photostationary steady state (PSS) and the ozone production efficiency (OPE) are calculated from airborne observations. A new metric, the oxidant production rate normalized to carbon monoxide (PRO*x*), is introduced and quantified as a function of the processing time of the plume. In most of the polluted plumes, it is found that the Leighton ratio (Φ) characterizing the equilibrium between O_3 and NO_x is, on average, within the PSS range ([1 ± 0.32]) or greater. The positive dependence of O_x to NO usually indicates a VOC-sensitive regime inside the plumes with some exceptions. In Paris, under oceanic westerly winds, and during DACCIWA, the plumes show a rural-like chemistry behaviour at moderate NO_x levels (NO_x-sensitive). Intense and frequent rapid changes in $J(NO_2)$, NO and NO_2 explain the deviations from the PSS. The OPE for Paris plume suggests that the VOC-sensitive regime extends far beyond the urban plume. The mean ozone production is higher downwind of Paris (30 ppb h^{-1} on average) compared to SWA (20 ppb h^{-1}) and WMB (6 ppb h^{-1}). PRO*x* values vary between 0 (no oxidant production) and 0.27 $ppb_{[Ox]}$ $ppb_{[CO]}^{-1}$ h^{-1}. The determined uncertainty on the Leighton ratio value could affect the differences in the estimation of the photochemical oxidant production by PO_3 and PRO*x*. The emissions of CO along the flight path and the presence of vegetation and high humidity levels might shape the oxidant production depending on the explored environment. While limited in number, PRO*x* values set a benchmark for future photochemical studies to compare with: Paris as representative of an anthropogenic urban plume and WMB as representative of a biogenic continental plume.

Received 9th November 2021
Accepted 16th April 2022

DOI: 10.1039/d1ea00093d

rsc.li/esatmospheres

Environmental significance

Tropospheric ozone is a secondary pollutant playing a key role in the oxidizing capacity of the atmosphere. While studied since the 80's, there are still pending questions on its budget given the heterogeneous distribution of its gaseous precursor emissions worldwide and the non-linearity processes involved in its production as recently recalled by the COVID-19 pandemic lockdown. Here we investigate the ozone–NO_y photochemistry in contrasting polluted plumes sampled by the Safire ATR-42 research aircraft over the last decade in the megacity Paris, North-West Mediterranean and southern West Africa urban areas. We use and discuss various metrics derived from the photostationary steady state and a new metric, PRO*x*, a CO-adjusted oxidant production rate. We show that the VOC-sensitive regime usually dominates inside the plumes and far beyond but with some exceptions regarding the environmental conditions. PRO*x* varies between 0 (no oxidant production) and 0.27 $ppb_{[Ox]}$ $ppb_{[CO]}^{-1}$ h^{-1} inside the plumes. PRO*x* values set a benchmark for future photochemical studies to compare with.

[a]*Université Clermont Auvergne, CNRS, Laboratoire de Météorologie Physique (LaMP), F-63000 Clermont-Ferrand, France. E-mail: agnes.borbon@uca.fr*
[b]*University of Grenoble Alpes, CNRS, IRD, INP-G, IGE (UMR 5001), 38000 Grenoble, France*
[c]*Université de Paris and Univ Paris Est Creteil, CNRS, LISA, F-75013 Paris, France*
[d]*Univ Paris Est Creteil and Université de Paris, CNRS, LISA, F-94010 Créteil, France*
[e]*Laboratoire des Sciences du Climat et de l'Environnement (LSCE), CNRS-CEA-UVSQ, IPSL, Université Paris-Saclay, F-91191 Gif-sur-Yvette, France*
[f]*CEREA, Joint Laboratory Ecole des Ponts ParisTech/EdF R&D, 77 455 Marne la Vallée, France*

† Electronic supplementary information (ESI) available. See https://doi.org/10.1039/d1ea00093d

1. Introduction

Apart from being a greenhouse gas, tropospheric ozone (O_3) plays a central role in the oxidizing capacity of the atmosphere. In the remote atmosphere, ozone is the dominant indirect precursor of the hydroxyl (OH) radical through its photolysis leading to electronically excited $O(^1D)$, followed by its reaction with water vapor. Ozone also reacts with nitrogen dioxide (NO_2) to form the nitrate radical (NO_3), an important intermediate in nighttime chemistry. Finally, ozone is an oxidant by itself involved in the oxidation of double-bound alkenes.[1] Because ozone is an oxidant, it has an impact on human health and vegetation at elevated concentrations. Surface ozone induces respiratory problems and is associated with premature death.[2,3] Surface ozone also causes tree damage,[4] reduces photosynthesis and growth[5] and, therefore, crop yields.[6,7]

The surface ozone levels depend on (i) natural and anthropogenic ozone precursor emissions, (ii) the photochemical reactions that lead to ozone formation and destruction and the actinic flux that drives this chemistry (iii) the transport of ozone and its precursors away from the source by advection, convection and mixing, and (iv) the loss of chemical species *via* wet and dry deposition.[8]

In most studies, it has been shown that elevated concentrations of tropospheric ozone are due to the increase of its precursor emissions[9] (and references therein). As a consequence, many actions have been taken worldwide in order to reduce these emissions. Those precursors mainly originate from anthropogenic sources,[10–13] especially in urban areas.[14–17] The relationship between ozone and its precursor concentrations is usually represented by an ozone isopleth diagram, which plots the maximum O_3 concentrations as a function of the initial VOC and NO_x concentrations.[18] This diagram enables three chemical regimes to be distinguished:

A standard regime: ozone production depends on both NO_x and VOC mixing ratios. The decrease in NO_x and/or VOC mixing ratios cause the decreases in ozone mixing ratios.

A NO_x-limited (or NO_x-sensitive) regime: NO_x mixing ratios are low and VOC/NO_x ratio is high (>15). Such a regime is usually found in rural areas. Ozone levels increase with NO_x levels and are little sensitive to VOC variations.

A VOC-limited (or VOC sensitive) regime: NO_x mixing ratios are high and VOC/NO_x ratio is low (<4). Such a regime is usually found in urban and suburban areas. Ozone levels decrease with or are insensitive to NO_x levels and increase simultaneously with VOC levels.

Policy to reduce urban air pollution has been typically developed by assuming that the chemistry is controlled by the VOC-limited regime. However, a recent study in Beijing by Newland *et al.*[19] shows that this simplistic separation of regimes is flawed. Indeed the authors observed that the NO_x-sensitive chemistry could even play a key role in central Beijing. Moreover, VOCs have both biogenic and anthropogenic origins, and the role of biogenic VOC (BVOC) emissions was demonstrated at the urban scale in Atlanta thanks to the seminal work of Chameides[20] followed by many others (see the review by Calfapietra *et al.*).[21] The authors showed that the reduction of ozone pollution is inefficient without considering the role of BVOC emissions in cities known to be high-NO_x chemical environments.

In response to the decrease in emissions of ozone precursors, several studies have shown that the surface ozone levels in summer are decreasing in the eastern United States[22–26] as well as in western Europe.[27,28] However, they may increase in the near future in urban areas because of a decrease in NO_x emissions due to traffic fleet renewal.[29] In contrast, in East Asia, several studies have reported either a decrease[30,31] or an increase in ozone levels[32–35] depending on the location. The wide range of trend values across urban and rural areas, especially for Europe, makes it difficult to describe an overall regional trend.[36]

The aforementioned observations highlight the non-linearity and the complexity of the relationship between ozone and the initial amounts of its precursors.[37] The reason for the decrease in ozone level in the post-industrialized world due to the reduction of its precursor emissions and its increase in the developing world are one of the main unanswered questions despite many years of research and substantial monitoring of the surface ozone at regional and global scales.[26] The Tropospheric Ozone Assessment Report (TOAR) **https://igacproject.org/activities/TOAR** (last access August 2021) has been addressing this question in North America, Europe, and East Asia[8,9,26,36,38–42] by first facilitating access to standardized ozone metrics for the determination of ozone production. However, this assessment is limited because of the heterogeneity of the data coverage. In the developing world like Africa, there is still a severe lack of observations. Therefore, a better understanding of ozone formation in contrasting regions of the world by applying a common approach is still needed.

In this study, we consider three international aircraft campaigns in contrasting regions in which the French atmospheric chemistry community has been involved during the last decade. These campaigns are relevant for the evaluation of photo-oxidizing capacity of the atmosphere: MEGAPOLI (Megacities: Emissions, urban, regional and Global Atmospheric Pollution and climate effects, and Integrated tools for assessment and mitigation; 2009; **http://megapoli.info**, last access August 2021),[43] ChArMEx/SAFMED (Chemistry-Aerosol Mediterranean Experiment/Secondary Aerosol Formation in the Mediterranean, in 2013)[44] and DACCIWA (Dynamics-Aerosol-Chemistry-Cloud Interactions in West Africa, in 2016)[45] in the Paris, North West Mediterranean, and southern West Africa regions, respectively. Those three regions encompass a diversity of environments in terms of ozone precursor emissions, emission regulation, urbanization, and photochemical conditions.[46–49]

Fig. 1 shows the multiyear evolution of ozone precursor's emissions since 2000 in those three contrasting regions. The annual emissions of NO_x and ethylene as representative of VOC precursors due to its elevated ozone-forming potential have been extracted from the global CAMS emission inventory (**https://permalink.aeris-data.fr/CAMS-GLOB-TEMPO**, last access August 2021). The following countries have been

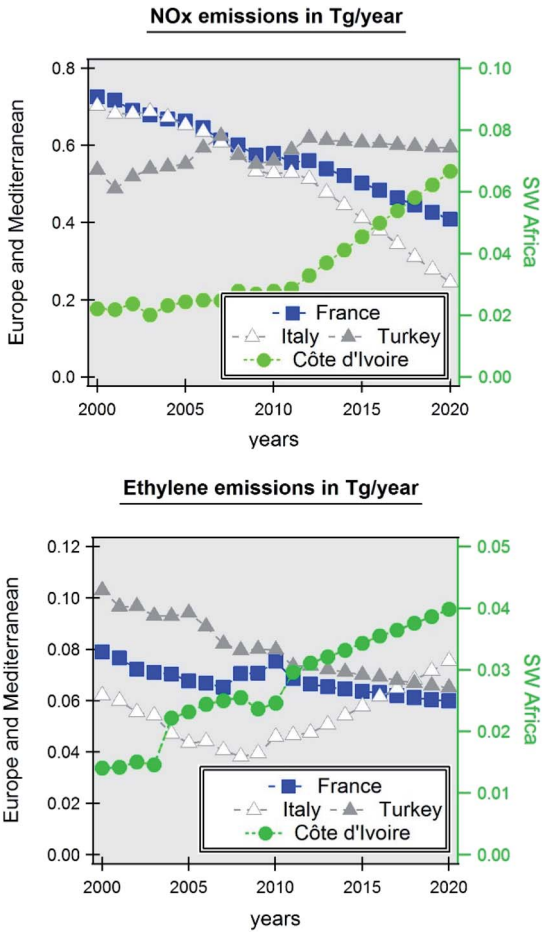

Fig. 1 Annual emissions of ozone precursors (upper panel: NO_x; lower panel: ethylene) from 2000 to 2020 in Europe (France), in the Mediterranean (Italy, Turkey) and in South Western Africa (Côte d'Ivoire). Emission data have been extracted from the CAMS emission inventory.[152]

selected: France for Western Europe, Italy and Turkey for the West and East Mediterranean, and Côte d'Ivoire and Ghana for southern West Africa. While there is a is a clear increase in anthropogenic emissions in SWA, the trends in Western Europe and in the Mediterranean are more contrasting depending on the species and on the country. On average a decreasing trend is observed.

The objective of this study is to provide an overview of the ozone chemistry in the polluted plumes transported in those three contrasting regions. There are numerous ways of studying the ozone photochemistry. The use of chemistry-transport models is one of them. However, modelling implies a good representation of the complex chemical and physical processes affecting the ozone distribution as well as the state of the atmosphere which varies from one location to another. As an alternative, metrics derived from observations have been widely used such as: the rate of ozone production,[50–54] quantification of the dynamic equilibrium between ozone and NO_x,[55–58] the estimation of the mixing ratios of peroxy radicals (RO_x) produced from the oxidation of VOC, CO and methane (CH_4)[56,59,60] and the efficiency of production of ozone.[61–64] These metrics give a hint on how ozone is formed and enable to access its relationship with its main precursors. They are calculated from the measurements of key species and are complementary to chemistry transport model outputs.

In this study, the analysis uses different metrics, focusing on the three summertime aircraft missions mentioned above, conducted over the last decade by the French ATR 42 environmental research aircraft of Safire. It starts with an introduction of the experiments (Section 2) followed by data selection and metric description (Section 3). Results (Section 4) are used to discuss the meteorological conditions, trace gas levels and variability before a comparative analysis of ozone and RO_x photochemistry and oxidant production.

2. Experiments

2.1. Aircraft campaigns

Fig. 2 maps the various aircraft flights from the three campaigns. The MEGAPOLI aircraft campaign took place in July 2009 (from 07/01/2009 to 07/29/2009) in the Paris area. The Safire ATR 42 was based at the airport of Cergy Pontoise North West of Paris (49.1° N, 2.0° E). The aircraft campaign was part of the European MEGAPOLI project aimed at investigating the interactions among megacities, air quality, and climate.[65] A total of 12 flights were performed in eight predefined sectors according to prevailing wind directions. During these flights, a complete circle around Paris and up to four transects perpendicular to the pollution plume at increasing distances from Paris center were performed.[66–68] The flight duration was about 3.5 hours and the maximum distance from the Paris center was 200 km. All the flights were performed in the afternoon at the maximum of photochemical reactivity and in a well-developed boundary layer height (500–700 m). A vertical sounding was performed at the end of the four transects.

The ChArMEx/SAFMED aircraft campaign took place in late July 2013 (from 07/24/2013 to 08/01/2013). The aircraft campaign was part of the ChArMEx program and aimed at assessing the physico-chemical state of atmospheric pollution in the western Mediterranean basin. The Safire ATR 42 was based at the airport of Genova in northwestern Italy (44.4° N, 8.8° E). The aircraft flew over a domain including the Ligurian Sea with the Gulf of Genova, the Tyrrhenian Sea, and the eastern coast of Corsica and Sardinia. A total of 6 flights (Fig. 2) including 3 vertical soundings over Ersa in Cape Corsica were performed. The maximum altitude ranged between 804 and 4207 m. As for MEGAPOLI, all the flights were performed during the afternoon at the maximum of photochemistry and lasted between 1 to 3.5 hours. In the following, they will be referred as SAFMED.

The DACCIWA aircraft campaign took place in June–July 2016 (from 06/29/2016 to 07/16/2016) during the monsoon season over the Gulf of Guinea and inland (incl. African countries like Ivory Coast, Ghana, Togo, and Benin). The DACCIWA international program aimed at studying the influence of anthropogenic and natural emissions on the atmospheric composition of southern West Africa and assessing their impact on human health, ecosystem and agricultural yield in a region where anthropogenic emissions are increasing.[69] A total of 20 flights were performed

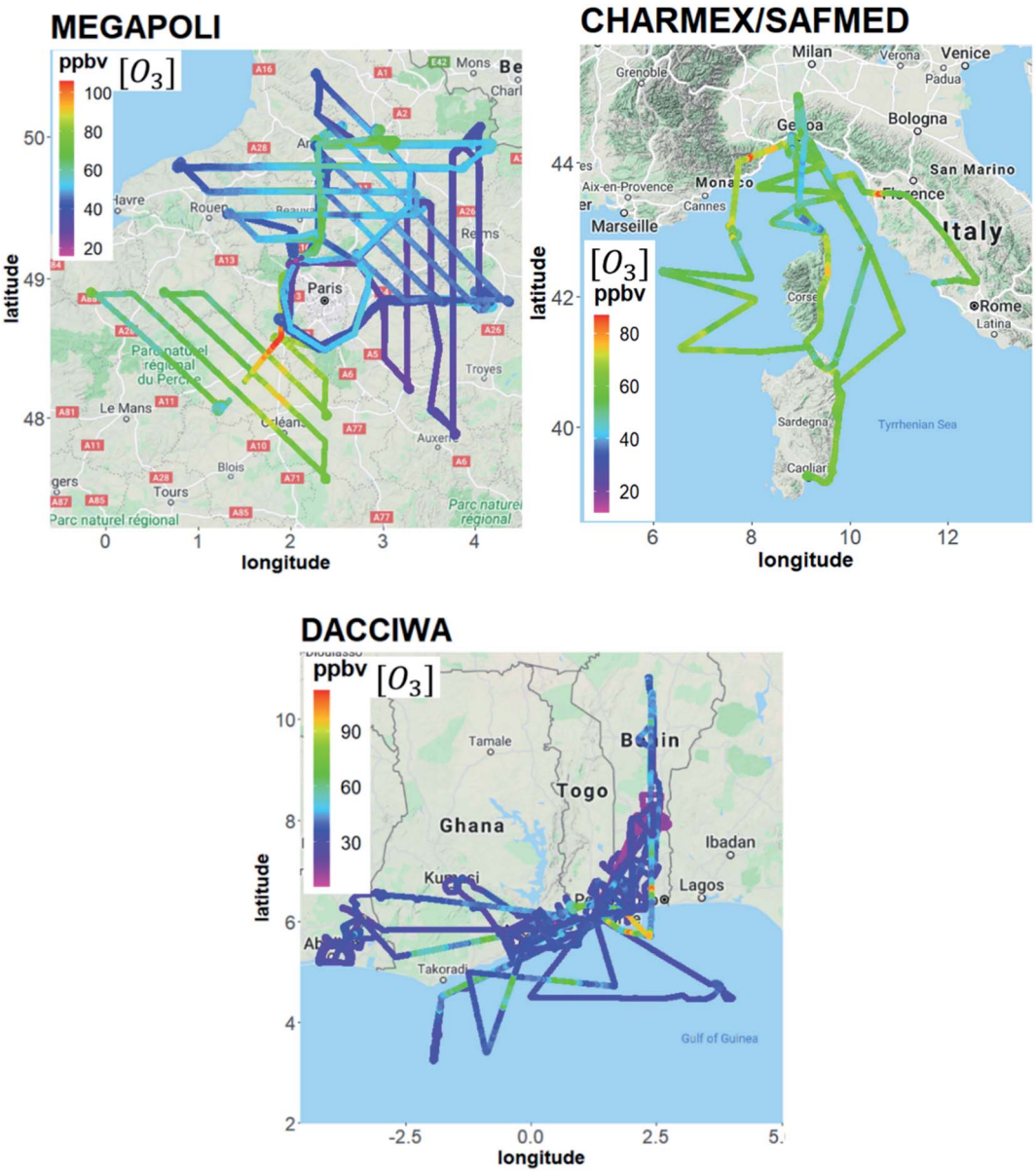

Fig. 2 MEGAPOLI, ChArMEx/SAFMED and DACCIWA aircraft flights color-coded by ozone mixing ratios in ppbv.

during morning and afternoon hours as plotted in Fig. 2. Detailed information about the DACCIWA aircraft campaign can be found in Flamant *et al.*[49] The sampling strategy generally consisted of two parts: first, vertical soundings were performed from 60 m up to 8 km above the mean sea level (a.m.s.l.) to identify relevant aerosol and trace gas layers. Subsequently, the identified layers were probed with *in situ* instruments by straight levelled runs at fixed flight altitudes. Urban plumes have been mostly sampled following the north-eastward direction which corresponds to the monsoon flux direction[70] downwind large urban conurbations such as Abidjan, Lomé, and Accra.

2.2. Chemistry instrumentation on-board the Safire ATR 42

The characteristics and performances of the instruments are reported in Table 1. Ozone and CO were sampled through a rear-facing 1/4 inch Teflon tube. During MEGAPOLI and SAFMED, ozone and CO were measured using ultraviolet and infrared analyzers (Thermo Fisher environmental instruments) with the MOZART instrument[71] based on the procedure implemented in the MOZAIC-IAGOS program.[72,73] The principle is based on the gas filter correlation of infrared absorption for CO and UV absorption for ozone. During DACCIWA, ozone was measured with a commercial analyzer (Thermo Environmental Instrument TEI49i UV photometric) and CO was measured with an analyzer based on cavity ring-down spectroscopy (CRDS) technology developed by PICARRO Inc.[74] During MEGAPOLI and SAFMED, nitrogen oxides (NO and NO_2) were sampled through a separate rear-facing pressure controlled inlet at a 30 s time resolution and measured using the MONA (Measurement of Nitrogen on Aircraft) instrument developed by the Laboratoire Interuniversitaire des Systèmes Atmosphériques (LISA).

Table 1 Physico-chemistry instrumentation deployed during the MEGAPOLI, SAFMED and DACCIWA campaigns

Species	Campaign	Technique	Time resolution	LOD	Accuracy (σ%)	References
Ozone (O_3)	MEGAPOLI, SAFMED	UV absorption (MOZART)	4 s	1 ppbv	5	Nedelec *et al.* (2005)[71]
	DACCIWA	UV absorption (TEI 49i)	1 s	1 ppbv	5	Brito *et al.* (2018)[70]
Carbon monoxide (CO)	MEGAPOLI, SAFMED	IR absorption (MOZART)	4 s	1 ppbv	5	Nedelec *et al.* (2005)[71]
	DACCIWA	CRDS analyzer (PICARRO Inc.)	1 s	4 ppb		Filges *et al.* (2015)[74]
Nitrogen oxides (NO, NO_2, NO_y)	MEGAPOLI, SAFMED	O_3 chemiluminescence photolytic converter (MONA)	30 s	10 ppt	10 20 13	Freney *et al.* (2014)[67]
	DACCIWA	O_3 chemiluminescence TEI 42iTL	20 s	50 ppt	20	Denjean *et al.* (2020)[82]
$J(NO_2)$	All	Chemical actinometry	1 s		10	Bohn *et al.* (2004)[75]

MONA consists of three NO commercial analyzers (Ecophysics CLD-780 TR). It measures NO_x (NO + NO_2) and NO_y (sum of NO_x and its oxidation products) concentrations by ozone chemiluminescence. NO is directly detected. NO_2 is converted into NO by a photolytic converter. NO_y is converted in NO by a gold converter heated at 200 °C with H_2. NO_y measurements were performed using a separate heated (60 °C) sampling line to avoid any loss of nitric acid. Additional details of the MONA instrument are given in the Supplement Material of Freney *et al.*[67] During the DACCIWA campaign, nitrogen oxides (NO_x) were measured by a TEI42 iTL chemiluminescence analyzer with a blue light photolytic converter which converts only NO_2 into NO.

The $J(NO_2)$ filter radiometer determines the rate of the *in situ* J_{NO2} photolysis in the atmosphere *via* a continuous measurement of the actinic flux in the appropriate wavelength of the 4 sr hemisphere. The filter radiometer is composed of two sensors measuring the downward and upward fluxes located above and below the aircraft's fuselage, respectively. The $J(NO_2)$ filter radiometer was calibrated at Jülich following the standard procedure as described in Bohn *et al.*[75] During the SAFMED aircraft campaign, upward $J(NO_2)$ data was not available. To deduce the total value of $J(NO_2)$ which is the sum of upward and downward $J(NO_2)$, the photolysis frequencies from the/SAFMED flights performed during summer 2014 (ref. 46) above the sea has been used. A relationship between upward and downward $J(NO_2)$ has been quantified (Fig. S1 in the ESI†). It was found that the maximum value of upward $J(NO_2)$ equals 10% of the value of downward $J(NO_2)$ (Fig. S1 of the ESI†). As a consequence, the following relationship was used for the 2013 SAFMED dataset to calculate the total value of $J(NO_2)$: $J(NO_2)_{total} = 1.1 \times J(NO_2)_{downward}$.

3. Methods

3.1. Data selection: searching for polluted plumes

3.1.1. Boundary layer height estimation. The objective here is to identify polluted plumes that develop in the boundary layer which is directly impacted by the emissions of ozone precursors at the surface. Only observations within the boundary layer will be selected in this study. The upper limit of the boundary layer has been defined through the examination of the vertical gradients of two physico-chemical parameters: relative humidity (RH in %) and ozone mixing ratios (in ppb) following Bechara *et al.*[77] The upper limit of the boundary layer is usually characterized by strong changes in the meteorological and pollution gradients. Since the boundary layer is a mixing layer, most of the photochemical reactions occur within that layer and most of the species are concentrated in this area. It can be visualized when there is a visible change in the RH (or humidity) and in the ozone vertical distributions. Fig. 3 shows the vertical distribution of RH (or humidity for MEGAPOLI campaign) and ozone for 4 selected flights during each of the three aircraft campaigns, whose patterns are representative of all flights.

In the Paris region, the vertical distributions of ozone and RH are quite homogeneous with a neutral vertical gradient along the first 2000 m indicating a well-mixed boundary layer in the mid-afternoon. Beyond 2000 m, the ozone and RH gradient becomes negative most of the time. This gradient shift signs the upper limit of the BL. This value is consistent with summertime and springtime observations inside (QUALAIR platform)[78] and outside Paris (SIRTA observatory located at 30 km in the South-West)[79,80] based on LIDAR measurements. The negative gradient of ozone suggests its photochemical production in the BL. In the West Mediterranean basin, the vertical distribution of RH and ozone reveals the presence of different layers. Di Biagio *et al.*[81] have already shown that the vertical distribution of aerosols and trace gases over the West Mediterranean presented a complex and highly stratified structure. While the upper limit of the marine boundary layer below 500 m is visible with a constant RH above 80%, the determination of the upper limit of the BL varies between 800 m (flight 51) to about 1000 m (other flights). This is in agreement with the height of the BL determined by Di Biagio *et al.*[81] In southern West Africa, the RH distribution shows a rather neutral gradient up to 1500–2000 m with values higher than 80%. Ozone is moderate and its distribution is homogeneous with some exception (flight 36). This corresponds to the wet monsoon layer characterized by a weak to moderate wind speed and a south-western flow. Above 1.5–2 km, the wind direction changes to the eastern sector and the wind speed increases. The atmosphere gets drier and ozone shows a positive gradient. The profiles and interpretation are

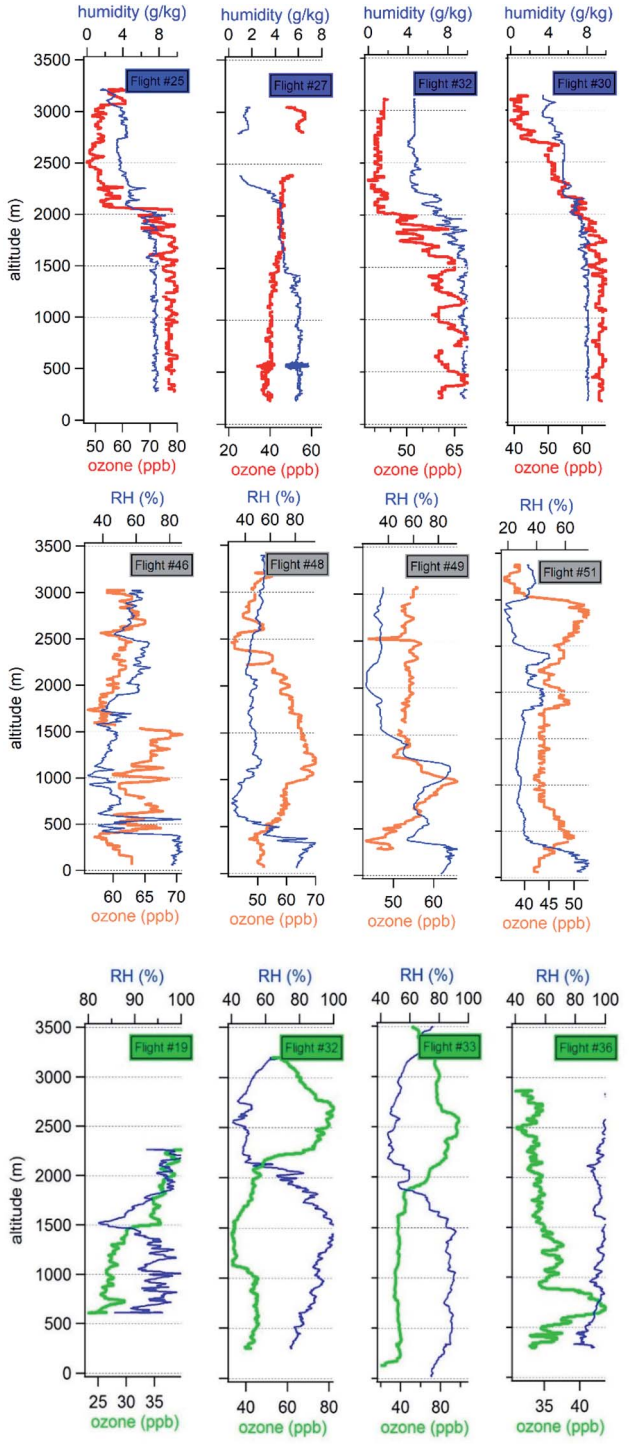

Fig. 3 Vertical profile of relative humidity (RH) and ozone during 4 flights from MEGAPOLI (blue, top plots), SAFMED (grey, middle plots) and DACCIWA (green, bottom plots) campaigns.

consistent with the vertical layering of aerosol and other meteorological parameters described by Denjean *et al.*[82]

To conclude, the change in the vertical distribution of RH and ozone is observed around 2000 m of altitude in Paris, 800–1000 m in WMB, and ranges between 1000 and 2000 m in SWA. In the following, only observations within the boundary layer will be taken into account.

3.1.2. The identification of the plumes. The identification of the polluted plume is based on the use of one short-lived chemical tracer (here NO_x) and wind direction to verify air masses are located downwind main source areas. Any remarkable increase of NO_x above their background regional levels consistent with wind direction is used as an indicator of plume crossing. In addition, the nature of the polluted plume (urban or biomass burning-type) has been identified, especially in SWA by using the ratio NO_x to CO as discussed in Denjean *et al.*[82] All the identified plumes for this study are urban (NO_x to CO ratio >1).

The time series of NO_x concentrations for each flight are examined in order to detect significant changes in NO_x concentrations above background levels. Fig. 4 reports the time series of NO_x (left axis) and ozone (right axis) for one representative flight of each campaign. The significant increase of NO_x levels above their background levels is remarkable in Paris each time the aircraft meets the urban plume. This feature is consistent with the increase of other anthropogenic ozone precursors like aromatic hydrocarbons as described in Borbon *et al.*[66] While less remarkable and frequent due to aircraft trajectory, the increase of NO_x is visible during DACCIWA and SAFMED. Regardless of the flights, the NO_x peaks correspond to a decrease of ozone within the plumes due to its titration by NO. In Paris and SWA, the NO_x increase is observed downwind the urban area. During SAFMED, flights 51 and 48 (not shown) were performed in the southern sector of Genoa. However, the NO_x levels during those flights did not show any consistent spatial gradient compared to Paris. The analysis of wind direction and the calculation of four back-trajectories for four hours using the HYSLIPT model[83] revealed a western wind regime. As an alternative, the round-trip flights 46 and 47 were chosen to capture the plume travelling downwind Corsica Island. Indeed, flight 46 flew over Genoa and Cagliari along the Corsica coast while the return flight flew over the Tyrrhenian Sea 50 km east away from flight 46. Fig. 5 shows the trajectory of the combined flight color-coded by the altitude and the trajectory of the air mass computed with HYSPLIT. The flight path has been color-coded with ozone because the NThe western origin of the winds on the whole domain implies a dynamical connection between air masses sampled by both flights. Only data measured between 785 and 806 m altitude corresponding to the BL region were selected based on the vertical sounding of flight 46 (Fig. 3). We also assume that the marine emissions of ozone precursors when air masses travel towards the East are negligible.

Since the photolysis rate of NO_2 used for the metric calculation in this study (see Section 3.2) is directly linked to solar radiation, it can easily be altered by the presence of clouds or aerosols. Thus, another criteria is clear sky conditions as quantified by a value of $J(NO_2)$ greater than 0.006 s^{-1}.[84,85] We filtered out all the data having a value of $J(NO_2)$ less than 0.006 s^{-1} during DACCIWA and SAFMED campaigns flights. There were only very few values of $J(NO_2) < 0.006$ s^{-1} over Paris even though the aircraft campaign took place most of the time under cloud cover. Therefore no filter has been applied to $J(NO_2)$ for MEGAPOLI.

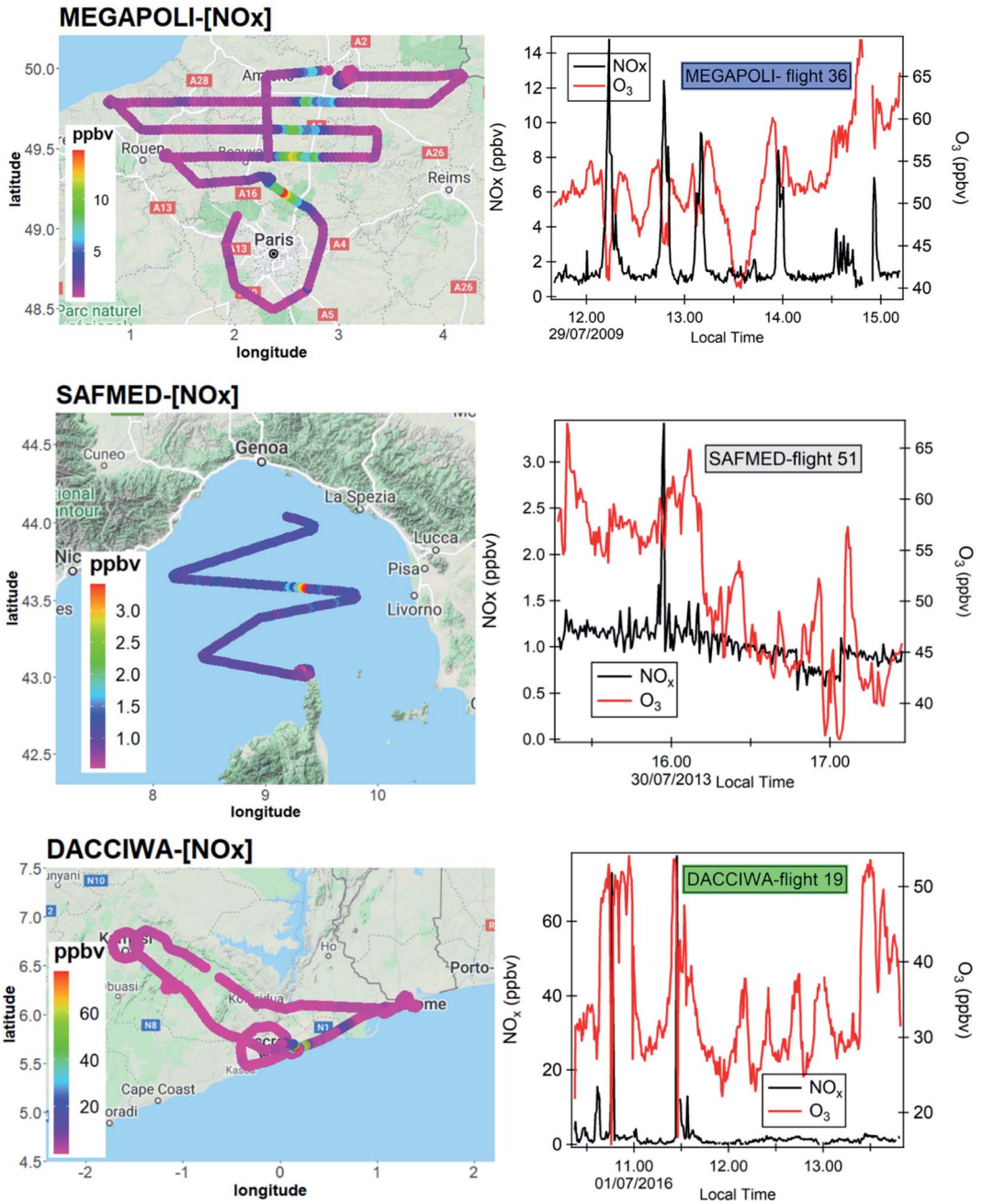

Fig. 4 Flight trajectories color-coded by NO_x mixing ratios during the MEGAPOLI, SAFMED and DACCIWA aircraft campaigns (left side) and corresponding time series of NO_x and ozone mixing ratios (right side).

During MEGAPOLI, SAFMED, and DACCIWA six, two (combined flights 46 and 47) and three flights met the above criteria, respectively. Table S2 in the ESI† shows the selected flights as well as their date and time, geographical sectors, and ozone pollution level.

During MEGAPOLI, flights sectors were South-West (SW) (flight 25), North (N) (flights 30, 32, and 36), and East (E) (flights 27 and 33). There was an important pollution level of ozone during these flights (52 to 73 ppbv on average) apart from the flights in sector E for which ozone levels were quite low (31 and 39 ppbv on average). All the flights took place between 11 : 00 and 17 : 00 at maximum sunlight hours favoring photochemistry. During SAFMED, flights 46 and 47 show an important level of ozone pollution with a mean mixing ratio of 63.7 ppbv. All DACCIWA flights were performed in cloudy conditions at low ozone pollution levels (34–37 ppbv on average). Even though $J(NO_2)$ has been filtered, these data should be used with care because filtering $J(NO_2)$ might not be sufficient.

3.2. Metrics

3.2.1. The Leighton ratio. Together with VOC, NO_x (NO_2 + NO) are the most important tropospheric ozone precursors.[86]

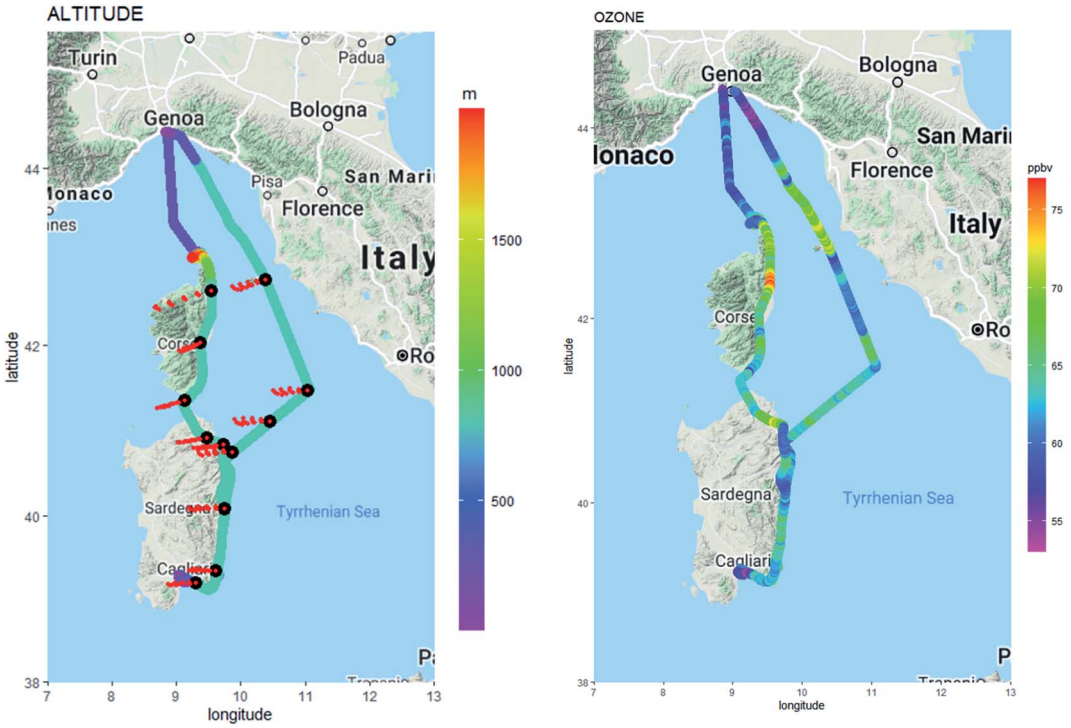

Fig. 5 Flights 46 and 47 selected for SAFMED color-coded by the altitude and back-trajectories (left-hand panel) calculated with HYSPLIT in red (Stein *et al.*, 2015)[83] and color-coded by ozone mixing ratios (right-hand panel).

During the daytime, a molecule of NO_2 is degraded photochemically to form a molecule of NO and an oxygen atom (O) (R1). The atom of oxygen then reacts quickly with one oxygen molecule (O_2) in the presence of a third body (M) to form O_3 (R2). That latter ozone molecule then quickly reacts with the NO to reform NO_2 and O_2 (R3).

$$NO_2 + h\nu \ \ (\lambda < 420 \ \text{nm}) \xrightarrow{k_1} NO + O(^3P) \qquad (R1)$$

$$O(^3P) + O_2 + M \xrightarrow{k_2} O_3 + M \qquad (R2)$$

$$O_3 + NO \xrightarrow{k_3} NO_2 + O_2 \qquad (R3)$$

k_1 corresponds to $J(NO_2)$ and comes from measurements, k_2 and k_3 are the kinetic constants of the reactions (R2) and (R3), respectively.

Reactions (R1) to (R3) are really fast leading to a steady-state within $\approx$100 seconds during daytime[55] and represent a null cycle in which no additional ozone is formed. The dynamic equilibrium between O_3–NO–NO_2 is known as the photostationary steady-state (PSS) and is quantified by the Leighton ratio Φ[87] expressed as follows:

$$\Phi = \frac{J_{NO_2}[NO_2]}{k_3[NO][O_3]} \qquad (1)$$

where $J(NO_2)$ (s^{-1}) (k_1) is the photolysis rate of NO_2 which depends on the solar irradiance. The brackets represent the molecular density concentration (in molecule per cm^3) of NO_2, NO and O_3. k_3 is the rate constant of the reaction (R3) and equals $3.10^{-12} \exp\frac{-1500}{T}$ cm^3 per molecule per s.[88] Since k_3 depends on the temperature, it has been calculated based on the temperature conditions encountered during the three aircraft campaigns and reported in Table S3.† When the steady state is assumed, O_3 concentrations can be predicted as follows:[88]

$$[O_3]_{PSS} = \frac{J_{NO_2}[NO_2]}{k_3[NO]} \qquad (2)$$

Φ equals (or is similar to) unity when reaction (R3) is the only (or the major) pathway of converting NO to NO_2 (PSS condition). Such case is usually observed in polluted urban areas under high-NO_x conditions.[51,56,58–60]

When the value of Φ is less than unity, the PSS conditions did not have time to be reached due to perturbations on the air mass like a rapid change in $J(NO_2)$ and in NO concentrations.[89]

Φ deviates positively from unity when other chemical pathways besides reaction (R3) convert NO to NO_2. Rapid changes in $J(NO_2)$, NO and NO_2 is another cause (see Section 4.3.1). The effect of other chemical pathways is observed under clean or moderately polluted conditions like rural and remote regions.[55,57,90–93] One major pathway is the reaction between NO and the peroxy radical (RO_x) that can be either organic (RO_2) or hydro (HO_2) following the reactions (R4) to (R6).

$$NO + HO_2 \xrightarrow{k_4} NO_2 + OH \qquad (R4)$$

$$NO + CH_3O_2 \xrightarrow{k_5} NO_2 + CH_3O \qquad (R5)$$

$$NO + RO_2 \xrightarrow{k_6} NO_2 + RO \quad (R6)$$

Reactions (R4) to (R6) are followed immediately by NO_2 photolysis (reaction (R1)) which will result in net O_3 generation. In the presence of an important concentration of peroxy radicals the Leighton ratio formula becomes:

$$\Phi = 1 + \frac{(k_4[HO_2] + k_5[CH_3O_2] + \sum k_6[RO_2])}{k_3[O_3]} \quad (3)$$

where k_4, k_5, and k_6 are, respectively, rate constants for reactions (R4) between NO and HO_2, (R5) between NO and CH_3O_3, and (R6) between NO and RO_2. k_4 and k_5 values are taken from Seinfeld and Pandis (2016)[94] and are equal to $3.310^{-12}\exp^{\frac{270}{T}}$ cm^3 per molecule per s, respectively. Values of k_3 and k_4 are reported in Table S3† for the selected flights. k_6 values apply for a variety of organic rests.

Since the rate constants k_4, k_5 and k_6 are relatively similar,[95] the Leighton ratio formula in remote or rural areas can be approximated as follows:

$$\Phi = 1 + \frac{k_6[RO_x]}{k_3[O_3]} \quad (4)$$

The uncertainty of the Leighton ratio, as experimentally derived from eqn (1), can be estimated by using the formula of the Gaussian error propagation as used in Hauglustaine *et al.*,[91] Mannschreck *et al.*,[57] and Trebs *et al.*[85]

$$\sigma_\phi = \sqrt{\sum {\sigma_i}^2} \quad (5)$$

where i is the parameter of each PSS ratio which are $J(NO_2)$, NO_2, k_3, NO and O_3. Each σ is taken from Table 1 and the uncertainty for k_3 was estimated to be 20% according to Atkinson *et al.*[97] An overall uncertainty of 32 % (1σ) for Φ was found for the MEGAPOLI and DACCIWA campaigns and 42% (1σ) for the SAFMED campaign.

3.2.2. RO_x mixing ratio derived from PSS. Peroxy radicals can be formed as products of reactions of the hydroxyl radical (OH) with carbon monoxide (CO), methane (CH_4), and non-methane hydrocarbons (NMHC), by reaction of O_3 or the nitrate radical (NO_3) with VOC and reduced sulfur species and by the decomposition of peroxyacetyl nitrates (PAN).[98–101] The Leighton ratio formula can be used to estimate total peroxy radical concentrations following eqn (6):

$$[RO_x] = (\Phi - 1)\frac{k_3[O_3]}{k_6} \quad (6)$$

Numerous studies have applied the PSS in order to estimate peroxy radical mixing ratios.[51,91,102,103] In those studies, authors found disagreement between $[RO_x]$ estimated from the PSS formula and total observed and modelled $[RO_x]$ by up to a factor of 2 to 3. The reasons for these disagreements are similar as those found in the deviation from the PSS: rapid changes in $[RO_x]$ calculation terms, cloud coverage and data uncertainties, potentially amplified by error propagation. Despite those disagreements, this metric is useful for comparison and can still give a hint on peroxy radical mixing ratios.

3.2.3. Ozone production rate (PO_3) derived from PSS. The ozone production rate (PO_3) is one of the most common metrics of atmospheric ozone-forming oxidation cycles. It is deduced from the (R1)–(R5) equations and by assuming NO is in steady state:

$$PO_3 = J_{NO_2}[NO_2] - k_3[NO][O_3] \quad (7)$$

here, it can be seen that (R4), followed by (R1) and (R2), effectively represents a path for producing ozone. In this treatment we have assumed that the only "additional" species oxidizing NO besides ozone are HO_2 and RO_2.

3.2.4. Ozone production efficiency (OPE). The ozone production efficiency (OPE) is another metric of atmospheric ozone-forming oxidation cycles. It represents the number of molecules of ozone produced per molecule of NO_x oxidized.[104] NO_x is a catalyst that can produce several molecules of O_3 before it is removed from the atmosphere by oxidation reactions. Several studies have determined OPE as the slope of the correlation between O_x (=O_3 + NO_2) and the total reactive nitrogen (NO_z).[37,105] O_x is used instead of O_3 because O_x is more conservative and it is not affected by the titration by NO (R3). NO_z is known as the difference between NO_y (sum of all odd-nitrogen compounds) and NO_x. It includes nitric acid (HNO_3), peroxyacetylnitrate (PAN), peroxynitric acid (HNO_4), and other organic nitrates.[88] This term was first defined by Liu *et al.*[37] which determined OPE at a rural mountain site in Colorado (USA) by using a photochemical box model. Later, Trainer *et al.*[105] determined OPE as the slope of the correlation between O_3 and NO_z mixing ratios from atmospheric observations. Since then, OPE has been widely determined in low NO_x areas (*e.g.*[105–107]) and in high NO_x urban plumes (*e.g.*[61,108–110]).

3.2.5. A new metric: the CO-normalized oxidant production rate (PRO*x*). The ratio $\Delta O_3/\Delta CO$ has been used to characterize the photochemical production of ozone in continental plumes during their long-range transport.[111,112] The parameter O_x (=O_3 + NO_2) has often been used to quantify the net photochemical formation of O_3 beyond its rapid daytime interconversion with NO_2.[50,113] NO_2 is included because it acts as a reservoir of O_3, formed by (R3) or as a source of O_3 (R4) and (R6). Here, a CO-normalized oxidant production rate or PRO*x* is established in order to quantify the efficiency of the photochemical production rate inside the plume. PRO*x* is defined as the ratio ($\Delta[O_x]$-to-$\Delta[CO]$) $\frac{\Delta[O_x]}{\Delta[CO]}$ as a function of the processing time. $\Delta[X]$ is the difference between the mixing ratios of X (O_x or CO) inside the plume and the X (O_x or CO) background value outside the plume. CO is a relatively unreactive tracer of dilution. The processing time does not exceed 10 hours. The residence time of CO ($k_{OH} = 1.44 \times 10^{-13}$ cm^3 per molecule per s) for an OH concentrations of 10^7 molecule per cm^3 (upper limit) roughly equal 8 days which is much higher than the average processing time. Normalizing by CO provides a dilution-adjusted oxidant production similar to the one of the organic aerosol to CO used in numerous studies.[114,115] It is assumed that

there is no additional CO emissions or ozone and CO loss along the plume track. This assumption will be examined on a case-by-case basis in Section 4.3.5. The processing time (in hours), defined in Brito *et al.*,[70] is the distance from the upwind urban center divided by the integrated wind speed along the flight trajectory. It is a proxy of the plume aging. The mean ratio $\Delta[O_x]$-to-Δ[CO] is calculated for each plume transect and plotted as a function of the processing time. PRO*x* (in $ppb_{[Ox]}$ $ppb_{[CO]}^{-1}$ h^{-1}) is derived from the slope of a piecewise linear regression fit between $\frac{\Delta[O_x]}{\Delta[CO]}$ and the processing time. PRO*x* integrates the temporal evolution of the net photochemical production. Here,

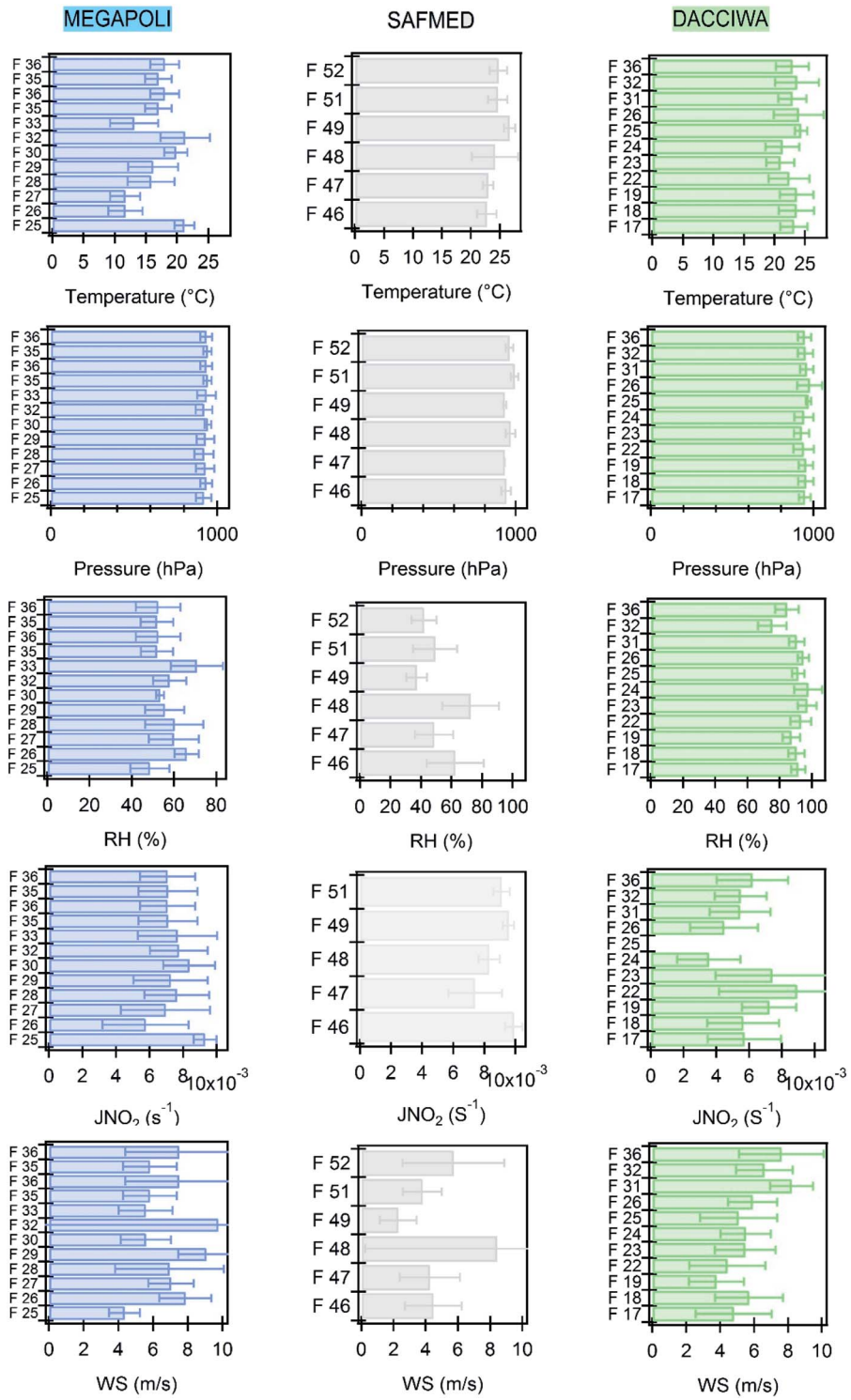

Fig. 6 Averages and their standard deviations of key meteorological parameters during the MEGAPOLI, SAFMED and DACCIWA's flights (temperature, pressure, relative humidity – RH –, photolysis frequency – J_{NO_2} – and wind speed).

the processing time does not exceed 10 hours. The residence time of CO ($k_{OH} = 1.44 \times 10^{-13}$ cm^3 per molecule per s) for an OH concentrations of 10^7 molecule per cm^3 (upper limit) roughly equal 8 days which is much higher than the average processing time. The loss of CO can be neglected.

4. Results

4.1. Meteorological conditions

Average meteorological parameters for all flights are reported in Fig. 6. The mean temperature in the Paris plume rarely exceeds 20 °C on average and varies over a large range from 11.7 °C (eastern sector) to 22.2 °C (northern sector). These values are consistent with ground-based temperature reported by Ait-Helal *et al.*[80] at the SIRTA observatory during the same period in Paris. Mean temperature gets higher towards lower latitudes from 20 °C to 25 °C on average and remains relatively constant between flights with an average temperature of 23 to 28 °C in the WMB and 20 to 24 °C in SWA.

Different wind regimes were encountered during MEGAPOLI as described in detail by Zhang *et al.*[116] Wind speed ranged between 4.3 and 9.1 m s^{-1}. The highest wind speeds were associated with westerly and southwesterly winds which bring fresher clean marine air masses to the region, mostly cloudy with rarely rainy conditions. A large range of wind speed values is also observed in SWA with average values ranging from 3.9 to 11.4 m s^{-1}. Wind speed is lower in the WMB with an average value of 4.5 m s^{-1}.

The relative humidity is the lowest in Paris with a maximum value of 54%. In the WMB and SWA, the relative humidity is larger, ranging between 52 and 62% and from 82 to 87% respectively. Higher relative humidity was found in SWA. This was predictable since the measurements took place during the wet monsoon season.

Average $J(NO_2)$ value ranges between 6.9×10^{-3} and 9.3×10^{-3} s^{-1} in Paris, 7.0×10^{-3} and 10^{-2} s^{-1} in the WMB, and 4×10^{-3} to 1.2×10^{-2} s^{-1} in SWA. Those values are consistent with the ones reported in previous studies at the same latitudes and seasons.[56,85,92,117,118] Finally, most of the flights took place under anticyclonic conditions favorable to photochemistry reactions. The positive gradient in temperature, humidity, and $J(NO_2)$ is consistent with the latitudinal gradient between the three regions.

Thus, these three regions are much contrasting in terms of meteorological conditions.

4.2. Trace gas mixing ratios per campaign

Fig. 7 shows the mean values of ozone, NO and NO_2 mixing ratios during the MEGAPOLI, SAFMED, and DACCIWA campaigns in the boundary layer. On average, the ozone levels are the lowest in SWA compared to mid-latitudes and are usually below 50 ppbv. The ozone levels show the highest variability in the Paris region probably due to changing meteorological conditions as discussed before. The ozone level is the highest during flight 25 in the south-eastern sector of Paris corresponding to stagnant and hot continental conditions: its level exceeds 70 ppbv. While Paris northern flights show similar ozone levels like the ones in the WMB (52 to 63 ppbv on average), the eastern flight ozone levels in Paris are in the same range as those measured in SWA (<40 ppbv).

The average observed ozone mixing ratios in Paris are in the same range as those measured recently in the London plume in the framework of the STANCO campaign (37 to 43 ppbv).[119] Compared to the ESQUIF aircraft campaign in Paris in 1998–2000, the observed ozone levels during MEGAPOLI are lower. During ESQUIF, average ozone mixing ratios were 65.5 ppbv with maxima of 109 ppbv but at that time, flights were preferentially performed under continental air masses after 2 to 3 days of stagnation in favor of the ozone accumulation.[120] It could therefore be compared to the highest ozone level we had during flight 25 (70 ppbv).

In the Mediterranean basin, the ozone level has been increasing in the last 20 years from 31 to 53 ppbv on a monthly average basis between 1998 and 2009.[121] The levels observed during SAFMED are within this range. Compared to the ESCOMPTE aircraft campaign along the Marseille-Fos Berre urbanized coast in southeastern France in 2001, ozone levels during SAFMED are lower (52 to 63 ppb). Indeed Coll *et al.*[122] reported that maximum mixing ratios of O_3 ranged between 80 to 160 ppbv.

In the framework of the AMMA project in the same region as DACCIWA, the ozone mixing ratio equaled 30 ± 10 ppbv on average in the lower troposphere with minimum values above forest regions where ozone deposition is enhanced by vegetation and reached up to 70 ppbv close to urban sites.[76,123] The levels found during DACCIWA are rather closer to regional background levels than the ones found in urban areas.

NO mixing ratios do not exceed 0.9 ppbv for all the three studied areas. However, SWA has the highest mixing ratio of NO (maximum value of 0.9 ppbv) followed by Paris (0.8 ppbv maximum) and WMB (0.6 ppbv maximum). NO_2 mixing ratios measured in Paris are twice as high as those measured in the WMB and in SWA with an average value ranging from 1.1 to 3 ppbv in Paris, from 0.6 to 1.2 in WMB, and from 0.3 to 1.7 in SWA.

4.3. Photochemistry

4.3.1. The Leighton ratio (Φ) and the photochemical steady state (PSS). The Leighton ratio has been calculated using eqn (1) for the MEGAPOLI, SAFMED and DACCIWA selected BL flights. The four terms in eqn (1) have been synchronized and averaged according to NO_x time resolution (20 or 30 s). Data with NO_x levels lower than 50 ppt (DL) have been excluded as low NO levels affect the calculation due to larger measurement uncertainty. It is found that Φ is usually within the PSS range ($[1 \pm \sigma]$) inside the urban plumes or higher. The effect of the uncertainty range on the results is discussed at the end of the paper. When Φ is within the PSS range, within the experimental uncertainty, O_3 is the only convertor of NO to NO_2. Outside the plume, except flight #25 during MEGAPOLI, Φ can reach values close to 10 in rural-like areas (*i.e.* flight 27 during MEGAPOLI). Higher values of the Leighton ratios outside the plumes were expected as shown in previous studies in remote areas.[58,85,92,96] In the following, the variability of the Leighton ratio based on the

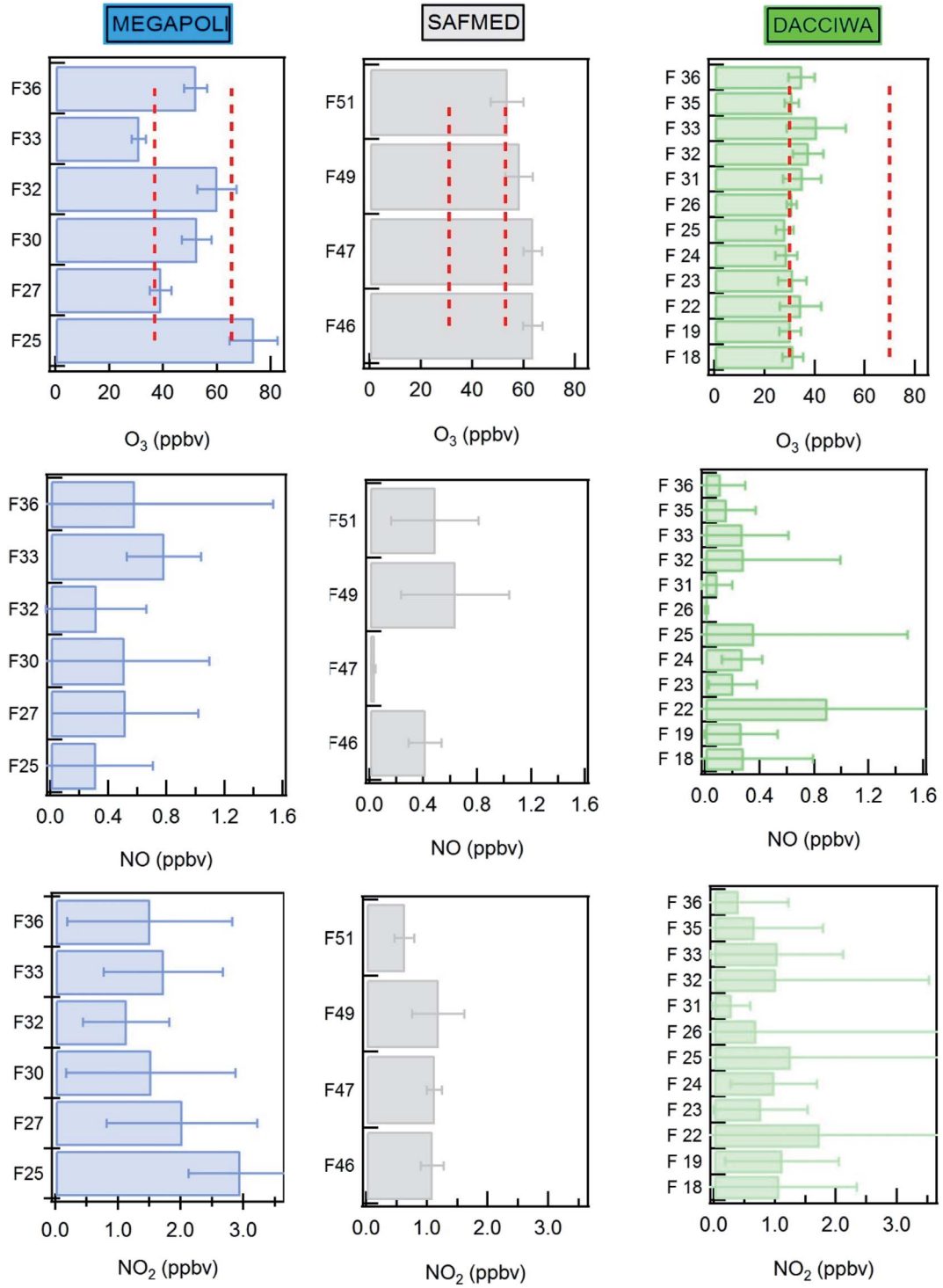

Fig. 7 Mean mixing ratio of ozone, NO and NO_2 during the MEGAPOLI, SAFMED and DACCIWA campaigns per flight. Red dotted lines are the range of ozone mixing ratios found in the literature (see text).

statistics reported in Table S4† is discussed per explored environment. Then, the influence of the rapid changes in the four terms in eqn (1), chemistry, and meteorology on this variability is examined.

Statistics on the deviations of Φ from unity. Various statistics on the Leighton ratio distribution are reported in Table S4:† the range (min and max) and average values of Φ during the whole flight and inside the plume, the percentage of data for which Φ negatively deviates from PSS ($<1-\sigma$) or positively deviates from PSS ($>1+\sigma$). The PSS is assumed to be reached within an interval at $\pm\sigma$. The uncertainty σ is calculated following eqn (5). We also investigated one of the reasons for those positive and

negative deviations by looking at rapid changes in the mixing ratios of the four terms: $J(NO_2)$, NO_2, NO and O_3 (see Section 3.2.1). Here, a rapid change is defined when the difference between two consecutive data is greater than 20% as suggested by Griffin *et al.*[58] Several studies have shown that the deviation from unity can be affected by rapid changes in the photo-oxidant concentrations and NO_2 photolysis rates[24,58,85,92] The rapid change in $J(NO_2)$ can be explained by the presence of clouds (*e.g.* in SWA) or the heterogeneity of the cloud cover (*e.g.* in Paris).

PSS during MEGAPOLI. During MEGAPOLI (6 flights), Φ values ranged from 0.41 to 3.93 in the Paris plumes. Except for flights 27 and 33, 53% to 90% of the values of Φ are within the $1 \pm \sigma$ interval. Flights 27 and 33 towards the eastern sector are characterized by much frequent and strong positive deviations of Φ from unity (>85%) and less than 13% of the data are within the PSS interval. One should note that both flights are characterized by lower mixing ratios of NO_x and O_3 compared to the other flights. This is a typical rural-like case usually encountered in moderately polluted conditions. The PSS is not reached within the plumes from 22% to up to half of the observations during flights 25, 32, and 36. The negative deviations from unity are most of the time explained by frequent and significant rapid changes between two successive measurements of $J(NO_2)$, NO, NO_2, and O_3 (Table S4† – 5th and 6th column). The magnitude of those changes reaches tens to several hundred percent (flights 27 and 33). The titration of ozone by fresh NO induced by the fast mixing of heterogeneous air masses is another reason that can be suspected in the time series in Fig. 4: at the maximum of NO loading in the plume, ozone dramatically drops down.

PSS during SAFMED. During SAFMED (2 combined flights), Φ ranged between 0.20 and 8.7. During flight 46, almost 90% of the values of Φ are within the $\pm\sigma$ interval while a systematic positive deviation from PSS is observed during flight 47 (between 4 and 8).

PSS during DACCIWA-SWA. During DACCIWA (3 flights), the Φ values range between 0.1 and 10.5 inside the urban plumes. Seventeen to 45% of the Φ values are within the PSS range while most of the data are higher than $1 + \sigma$ (Table S4†). As for MEGAPOLI and SAFMED, frequent and intense (several tens percent) rapid changes in $J(NO_2)$, NO, NO_2 and O_3 are responsible for positive and negative deviations of the Leighton ratio from unity.

Fig. 8 shows the average values of the Leighton ratios and the associated standard deviations found in the eleven investigated plumes compared to previous studies. Table S5† shows the aggregated Φ value from those previous studies. On average and despite the heterogeneous distribution of the Leighton ratio discussed above, the PSS is either reached within its lower and upper limits in half of the explored flights or overpassed during the eastern MEGAPOLI flights and the DACCIWA flights. One should note the high standard deviations displayed by the latter cases as reflected in the statistics in Table S4† (see statistics discussed above). There is a good agreement between this study and the previous ones in urban plumes or high NO_x environments. Apart from the value of Φ found in an urban plume in the Amazonas State in Brazil,[85] all the values of the Leighton ratios were within the PSS range of our study ([0.68–1.32]) and show a significant standard deviation.[60,89,124–126]

Chemical control on Φ. The dependence of Φ on [NO] mixing ratios and the PSS terms (namely, the products $J_{NO_2} \times [NO_2]$ and $([O_3] \times [NO])^{-1}$ from eqn (1)) has been investigated and is represented in Fig. 9 for one representative flight of each campaign. Complements are reported in Fig. S6 and S7 of the ESI† for all other selected flights. During MEGAPOLI and SAFMED, Φ usually decreases with increasing NO while it is less clear during DACCIWA. Moreover, the highest value of Φ does not correspond to the highest J_{NO_2} values as already described by Beygi *et al.*[127] in the marine boundary layer.

During MEGAPOLI (Fig. 9a), scatterplots show that Φ usually positively deviates from PSS values outside the plume (low NO_x), is close to unity on the edges of the plume, and lower than unity at higher NO_x. For flights 30 and 32 in the northern sectors, Φ

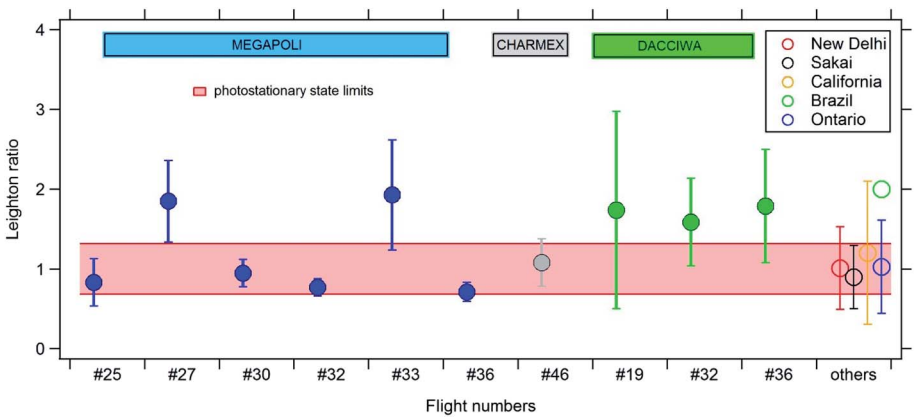

Fig. 8 Average Leighton ratio values (±standard deviation) calculated in the plumes of Paris (blue), WMB (grey) and SWA (green) (this study). The red shaded area is the photostationary range calculated in this study: [0.68–1.32]. On the right side, the values of the Leighton ratio from previous studies are reported: New Delhi, India (Masiwal *et al.*, 2019),[126] Sakai, Japan (Matsumoto *et al.*, 2006),[60] Claremont, California (Shetter *et al.*, 1983),[124] Amazonas State, Brazil (Trebs *et al.*, 2012)[85] and Ontario, Canada (Davis *et al.*, 2019).[125]

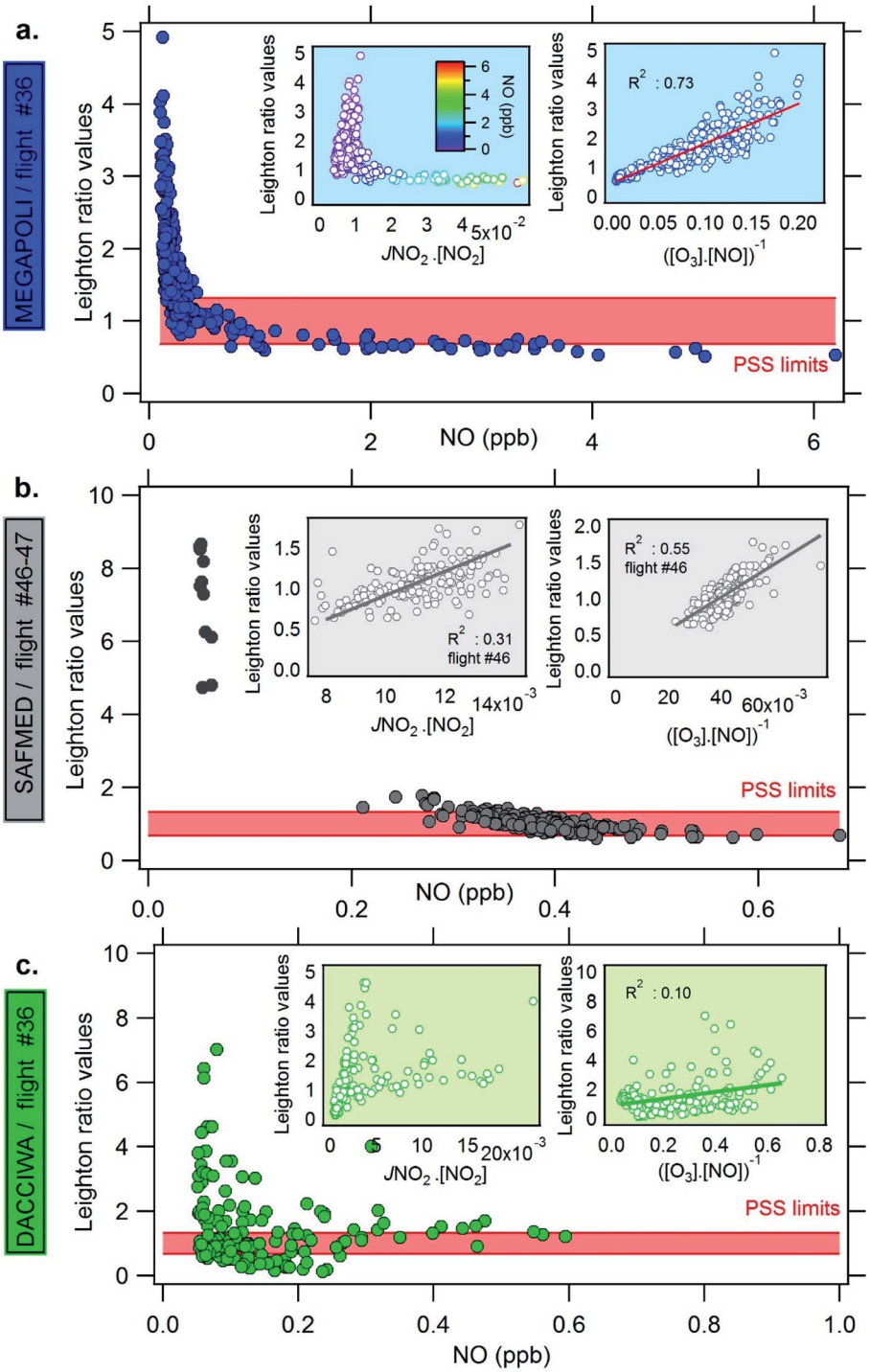

Fig. 9 Scatterplots of Φ *versus* NO mixing ratios during the three campaigns: flight 36 for MEGAPOLI, combined flights 46 and 47 for SAFMED and flight 36 for DACCIWA. Scatterplots are color-coded with $J(NO_2)$. The background-colored scatterplots represent the correlation of Φ with the PSS terms.

positively or negatively deviates from unity. The scatterplots between Φ and the two PSS terms reveal that the variability of Φ is mostly driven by $([O_3] \times [NO])^{-1}$ with a positive correlation, the latter explaining 73% of its variance. The same feature is displayed by other flights (R^2 ranging from 0.52 to 0.72) except during flight 33 where the correlation between both PSS terms is less clear (not shown here). During SAFMED (Fig. 9b), Φ displays a significant positive correlation with both PSS terms with an R^2 of 0.31 and 0.55, respectively. The products $J_{NO_2} \times [NO_2]$ and $([O_3] \times [NO])^{-1}$ both control the Φ variance. During DACCIWA (Fig. 9c), the dependence of Φ on both PSS terms is not as clear as for MEGAPOLI and SAFMED. No significant

correlation with the two PSS terms is depicted with an exception with flight 36 for which $J_{NO_2} \times [NO_2]$ explains 31% of Φ variability.

The positive deviations show that there are other pathways besides reaction (R3) converting NO to NO_2 such as the presence of peroxy radicals from the oxidation of VOC, CO, and CH_4.[57,58,127] Indeed, plot trajectories and time series analysis of the Leighton ratio show that maximum values of Φ are found near biogenic areas suggesting the influence of biogenic VOC and their oxidation products in the ozone production cycle[128] (Fig. S8† shows the case of flight 25 of MEGAPOLI campaign and 19 of DACCIWA campaign for which the highest deviations are observed). In addition to peroxy radicals, other reactions can convert NO to NO_2 such as halogen monoxides (XO where X represents a halogen atom-like I or Br). This case is mainly found in the marine boundary layer.[92,129]

Ozone mixing ratios have been estimated from the PSS inside the plumes following eqn (2) and compared to the ones from observations. For all explored environments, the predicted ozone equals observed ozone by ±40%. Finally, as expected, predicted ozone is well explained by the PSS formula inside the plume when the Leighton ratio is within the PSS range for all the contrasting regions.

Meteorological control on Φ. The dependence of Φ on meteorological conditions has been studied by assessing the correlation between the Leighton ratio values and the temperature, pressure, wind speed and direction, the relative humidity both for each flight and for all the flights combined per campaign. It is found that Φ doesn't depend on any meteorological parameters for any of the 3 campaigns (maximum correlation coefficient of 0.2). These results are in agreement with the work of Griffin *et al.*[58] at the University of New Hampshire Atmospheric Observing Station at Thompson Farm in the USA. One reason might be the relative stability of the meteorological conditions for the duration of one flight (4 hours maximum).

Conclusion on the Leighton ratio variations. In conclusion, PSS is reached on average in the plume except during eastern MEGAPOLI flights (NO_x-sensitive) and DACCIWA flights. This is consistent with the previous studies cited earlier. As a consequence, ozone levels are well predicted by the PSS inside the plume. Outside the plume, Φ deviates positively from unity suggesting the presence of other NO to NO_2 conversion pathways than O_3. Apart from the rapid changes of the species mixing ratios, sunlight intensity, and the presence of clouds,[58,85] other reasons for the deviations from the PSS can be the presence of inhomogeneous air masses bringing other precursors of ozone during the plume transport such as VOC of biogenic origin and even halogen monoxide (during the SAFMED flight for example). Meteorological parameters do not seem to influence the variability of the Leighton ratio given the short duration of each flight while the chemical control by $([O_3] \times [NO])^{-1}$ and to a lesser extent, $J_{NO_2} \times [NO_2]$ plays a role.

4.3.2. The peroxy radicals [RO_x] from PSS. The mixing ratios of [RO_x] have been estimated indirectly using the measured positive PSS deviations following eqn (6) during the 3 campaigns. This assumes that the deviation from the photostationary state relation from unity is related to the presence of peroxy radicals. The mean values of [RO_x] are reported in Fig. 10 (upper panel) inside and outside the plume. Table S6† shows the aggregated values of the maximum values of [RO_x]. The range of measured [RO_x] from the literature is also reported in Fig. 10.

[RO_x] mixing ratios are usually higher outside the plumes and lower inside except during flight 36 in DACCIWA on average. This is in agreement with the Leighton ratio calculations discussed previously. It suggests that there is almost no production of O_3 inside the plumes with higher NO mixing ratios and increased production of [RO_x] as long as we are getting further from the plumes.

While the mean [RO_x] mixing ratio barely reaches 29 ppt inside the plume during SAFMED (flight 46), the [RO_x] mixing ratios outside the plumes can reach more than a hundred of ppt in SWA and in the surroundings of Paris on average. The levels of [RO_x] in Paris and SWA are comparable. The calculated [RO_x] mixing ratios in the plumes are within the same range as those found in the literature: 10 to 50 ppt in Paris, 50 to 100 ppt in SWA, and 29 ppt in WMB. Results in the literature have shown [RO_x] mean mixing ratios of tens of ppt in remote rural environment (25–77 ppt),[55,91,130] in remote marine area (5–60 ppt),[55,59,91,131] in suburban Paris (maximum of 50 ppt)[132] and in an urban polluted area like in the city of Manaus in Brazil (15–60 ppt).[85] [RO_x] mixing ratios have reached 300 ppt in a rural area in Alabama.[90] In Paris, one should note that the calculated [RO_x] outside the plumes are greater than the ones measured at the SIRTA observatory in south-eastern Paris during MEGAPOLI by Michoud *et al.*[132] by a factor of 2 to 3 on average. Even though it has been found that estimation of peroxy radicals by the PSS method overestimates [RO_x] mixing ratio by up to 2 to 3 times,[90,91,96,103] some studies have found that the estimations of the peroxy radicals using constrained 0D box models are in better agreement with the measurements.[132–134]

The overestimation of RO_x by the PSS first suggests that there could be another reaction occurring that converts NO to NO_2 such as halogen monoxides or other unknown reactions.[85] Since [RO_x] and Φ are directly linked in eqn (6), their deviations are caused by similar reasons: uncertainties in all the terms used in the calculation, rapid changes in the measured species, a mixture of heterogeneous air masses, and the presence of clouds.[56,103] Even though the estimation of the peroxy radical mixing ratios is overestimated by the PSS method, it remains a relevant way to compare plumes in contrasting regions.

4.3.3. Ozone and ozone production rate in the PSS regime. The ozone production rate has been calculated according to eqn (7) and the mean values of PO_3 and their standard deviation are shown in Fig. 10 for the three regions inside and outside the plume.

The ozone production is either higher or lower outside the plumes except for flights within the PSS range (see Section 4.3.1). Outside the plumes, the mean ozone production ranges between 8 and 76 ppbv h^{-1} in Paris, equals 6 ppbv h^{-1} in the WMB, and varies from 5 to 17 ppbv h^{-1} in SWA. Paris shows the highest average ozone production. These estimations from eqn (7) are within the same range as those found in the literature (Fig. 10 – lower panel). Airborne studies estimating ozone

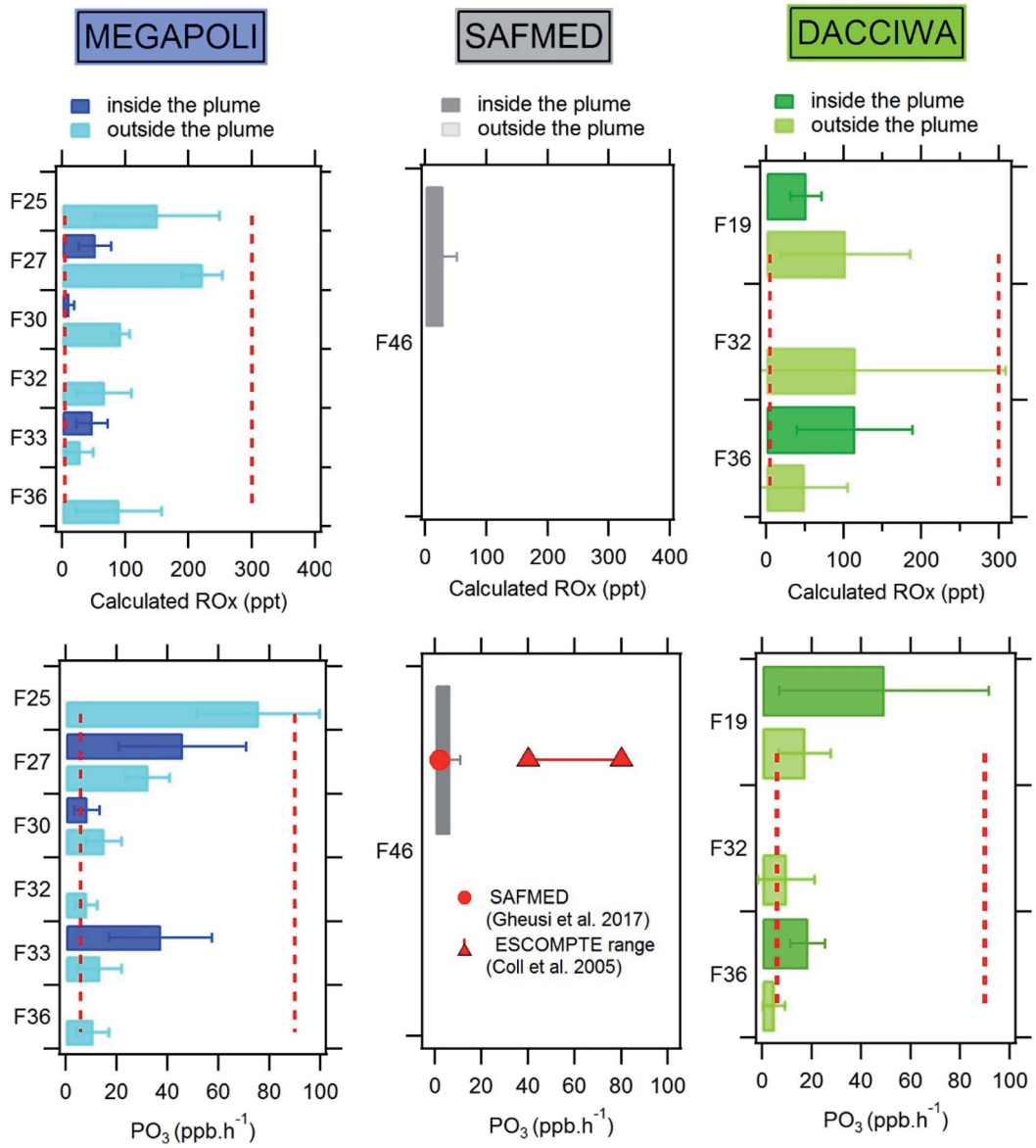

Fig. 10 Mean and standard deviations values of [RO_x] and ozone production (PO_3) calculated from the PSS in Paris, WMB and SWA. Dashed lines (for MEGAPOLI and DACCIWA) are the range of values reported in the literature in the same region (see text for references).

production inside urban plumes were most of the time conducted in North American cities: New York,[135] Atlanta,[136] Nashville.[137] The authors found that PO_3 ranged between 1 and 14 ppbv h^{-1}, 6–30 ppbv h^{-1} and 30 to 60 ppbv h^{-1}, respectively. In European cities such as Milan[138] and Berlin,[56] the PO_3 value could reach 50 and 90 ppbv h^{-1}, respectively. During SAFMED, the ozone production was also derived from boundary-layer pressurized balloon (BLPB) pseudo-Lagrangian flights over the WMB.[139] The reported range of 1 to 2 ppb h^{-1} is within the variability of the calculated PSS RO_x of 6.1 ± 4.4 ppb h^{-1}. This production remains by far lower than the estimation of 60 to 80 ppb h^{-1} made by Coll *et al.*[122] a decade ago downwind the urban area of Marseille and, consequently, closer to gaseous precursor sources.

Depending on the physical and chemical conditions, the production of ozone can be either NO_x-sensitive or VOC-sensitive. To investigate the chemical control on ozone production, Fig. 11 represents the scatterplot of the sum of oxidants ($O_x = O_3 + NO_2$) *versus* NO inside the plume during the MEGAPOLI flights. The ozone production efficiency (OPE) discussed in the next Section 4.3.4 will explore the chemical regimes outside the plumes. O_x decreases as a function of NO inside the plumes except for the eastern flights 27 and 33 during MEGAPOLI. For the latter, there is almost no trend. A similar negative dependence is depicted inside the DACCIWA plumes (not shown). During ChArMEx, no significant trend could be extracted (not shown). The Mediterranean area is in general NO_x limited during summer.[140] The negative trend for Paris and SWA indicates a VOC-sensitive regime with an exception for

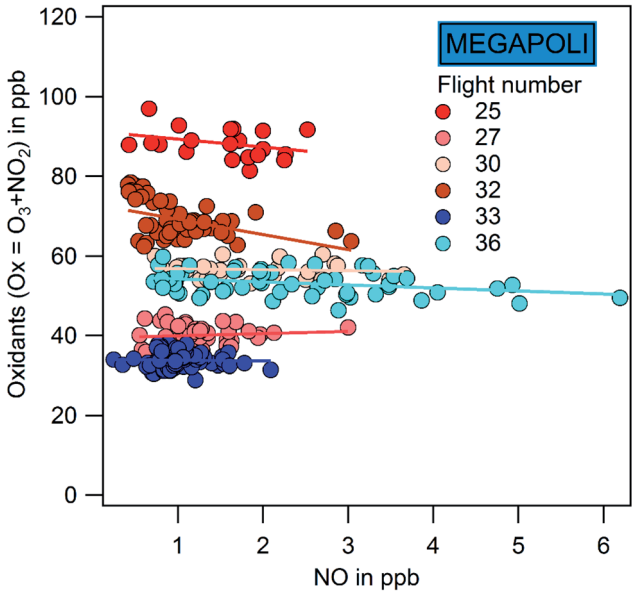

Fig. 11 Scatterplots of ozone and NO in the Paris plume during MEGAPOLI flights in Paris.

flights 27 and 33 in favor of a rather NO_x-sensitive regime. This is consistent with the Leighton ratio discussion.

4.3.4. Ozone production efficiency (OPE). The OPE described in Section 3.2.2 has been calculated as the slope of a linear least squares regression fit of the O_x *versus* NO_z scatterplot. The measurement of NO_z was not available during DACCIWA. One condition to derive the OPE from the slope of O_x *versus* NO_z is the statistical linear relationship between O_x and NO_z. During MEGAPOLI, it is found that there is no correlation between O_x and NO_z inside the plume (r^2 lower than 0.14). At this stage of the analysis, OPE suggests that there is little production of ozone inside the plume since the PSS is most of the time reached except during flights 27 and 33. During SAFMED, there is neither a correlation between O_x and NO_z. As a consequence, the OPE has been only derived from the MEGAPOLI flights outside the plume and compared to the literature. Results are reported in Fig. 12 (flight 32) and S15† (flights 25, 30, and 36). Flights 27 and 33 have been removed from this section since there is a lack of correlation between NO_z and O_x.

Values of OPE range between 4.6 and 6.9 with a coefficient of correlation r^2 between 0.33 and 0.53. These values lie within the ones reported in the literature as illustrated in Fig. 12a and in Table S20.† Usually, the OPE tends to be lower in urban areas compared to rural ones. In North American cities OPE is lower than 5. OPE values can be used as an insight on the O_3–VOC–NO_x sensitivity according to Sillman:[141] low OPE (<7) is linked to VOC-sensitive regime while high OPE (>7) is linked to NO_x-sensitive regime. By taking into account these criteria, one can conclude that the explored area outside the Paris plume is rather VOC-sensitive. However, the values close to 7 also suggest a transition regime between VOC and NO_x-sensitive as suggested by Sillman during ESQUIF.[142]

NO_x oxidation yields to the production of NO_z, and as a consequence, the NO_z mixing ratio is expected to increase when the O_3 production increases. OPE has been plotted against the maximum NO_x mixing ratio outside the plumes for all the MEGAPOLI flights (Fig. 12b). Apart from flight 25, OPE decreases with the increase in NO_x. This has also been observed in Liu *et al.*,[37] Ryerson *et al.*,[143] and Henneman *et al.*[144] Indeed the O_3 production is more efficient at low NO_x in terms of NO_x consumption,[104] because more OH reacts with VOC's instead of NO_2.

Table S7† shows aggregated values of OPE found in both rural and urban areas in previous studies. While OPE values are very variable from one location to another, it is globally lower than 7 in urban areas[104,135,144–146] and can go up to 10 in Beijing, China[147–149] or 18 in New York.[150] OPE is globally higher in rural low NO_x areas.

Previous studies have shown that OPE values deduced from observations could be overestimated.[61,151] Indeed, the relationship between the concentrations of O_3 and the products of the

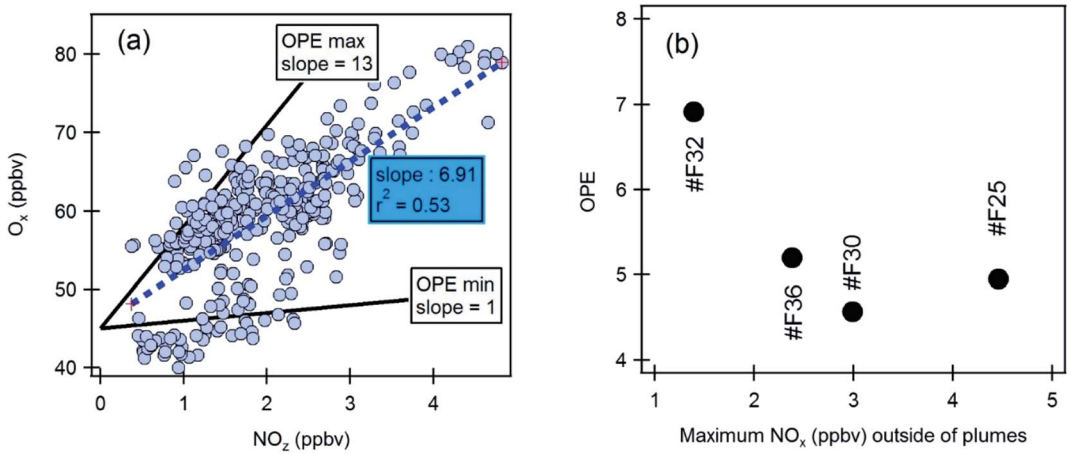

Fig. 12 Ozone production efficiency (OPE) during selected MEGAPOLI flights outside the plume. (a) Scatterplots of O_x (=O_3 + NO_2) *versus* NO_z during flight 32. The black lines are the range of the OPE values found in the literature and reported in Table S20.† (b) OPE for each flight *versus* maximum NO_x mixing ratio found outside the plumes.

NO_x oxidation must be shaped by the relative rates of chemical and depositional removal of O_3 and the NO_x oxidation products, and the transport processes that mix air parcels.

4.3.5. The CO-normalized oxidant production rate (PRO*x*). PRO*x* has been calculated in the Paris, WMB, and SWA plumes. The mean value and the standard deviation of $\Delta[O_x]/\Delta[CO]$ in each plume transect are reported in Fig. 13 as a function of the plume processing time for representative flights. The range of $\Delta[O_x]/\Delta[CO]$ values is consistent with the ones reported during long-range transport plume over the Pacific relying on the $\Delta[O_3]/\Delta[CO]$ variable (0.2 to 0.5).[111] Here, PRO*x* is derived from

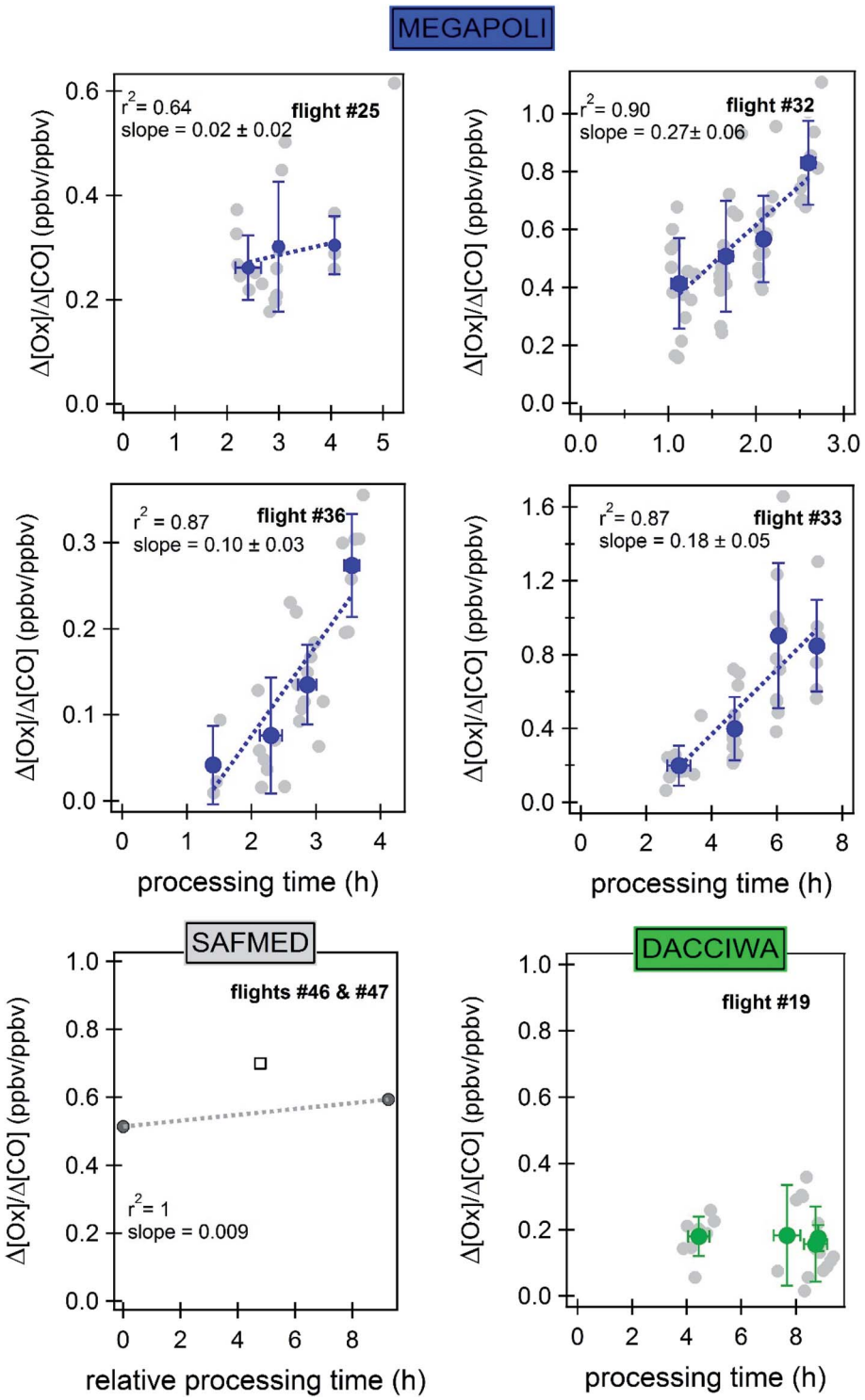

Fig. 13 Scatterplot of the production of oxidants with the processing time inside urban plumes in Paris (MEGAPOLI), WMB (SAFMED) and SWA (DACCIWA). The mean and standard deviations inside each plume leg are also reported (colored points and bars).

the slope of the piecewise linear fit. The calculated processing time spans from 1 to 8 hours.

In Paris, $\Delta[O_x]/\Delta[CO]$ linearly increases with the processing time ($r^2 > 0.80$), except for flight 30 (Fig. 13). PRO*x* varies between 0.11 to 0.27 ppb_{Ox} ppb_{CO}^{-1} h^{-1} in Paris while it is close to zero during flights 27 and 30. In other words, 0 to 0.27 ppb of oxidants are produced per ppb of emitted CO per hour in the explored polluted plumes. After 6 hours the oxidant production is still efficient (flight 32). The maximum PRO*x* is estimated during the northern flight 32. During this flight, ozone pollution levels have been qualified as high (Table S2†) as for flight 25. However, during flight 32, the average ambient temperature and the wind speed were the highest compared to flight 25 with low wind speed conditions. These conditions imply an efficient transport and photochemical production of the ozone precursors freshly emitted from the Paris urban area up to 200 km away.

During the SAFMED combined flights, $\Delta[O_x]/\Delta[CO]$ also increases with the processing time with a PRO*x* of 0.009 ppb_{Ox} ppb_{CO}^{-1} h^{-1}.

During DACCIWA, there is no increase in $\Delta[O_x]/\Delta[CO]$ as a function of the processing time for any of the selected flights (Fig. 13 for flight 19): PRO*x* is zero. The map of flight trajectories (Fig. S8† and 4) has shown that the aircraft flew over vegetation areas which could favor the dry deposition of ozone on leaves. Furthermore, SWA is characterized by a dense cloud cover and high relative humidity (>90%) which could also enhance the wet deposition.

Finally, sink (ozone removal by dry/wet deposition, CO oxidation) and source terms like the emission of CO along the flight trajectory could shape the PRO*x*. We discuss here the effect of potential emissions of CO along the flight tracks and how it affects the ΔCO term. In addition to its direct anthropogenic origin, CO can be also emitted by natural sources as already described in the literature: a direct oceanic source[153] and its photochemical production from the oxidation of biogenic VOC.[154,155] The potential oceanic source can be neglected during the SAFMED flight as it may not affect the ΔCO term, the potential marine source contribution being included in the background CO term. The MEGAPOLI flights were designed in order to cover the region beyond the whole Ile de France urbanized area where anthropogenic emissions concentrate. Moreover, the background signal levels outside the plume are clearly lower than the ones inside the plumes suggesting that the emissions from the surrounding areas can be neglected. For DACCIWA we cannot exclude the effect of CO emissions during the flight trajectory. Moreover the analysis of the mixing ratio distribution did not reveal any sudden increase of CO during the flights or any variation in its background levels during one single flight. Regarding its biogenic photochemical origin from BVOC oxidation, the homogeneity of the background CO levels outside the plumes suggest that there is no specific biogenic emission signature and, at worse, it is included in the background estimation. However one cannot exclude that biogenic VOC oxidation fuels the O_x production inside the plume.

The values of PRO*x* have been compared to the ones derived from the investigation of the ozone transboundary polluted plumes in East Asia by Cuesta *et al.*[156] From their $\Delta[O_3]/\Delta[CO]$ variable, we derived a PRO*x* equivalent over a six-day period. A value of roughly 0.001 ppb_{O3} ppb_{CO}^{-1} h^{-1} is found. This value is one order of magnitude lower than the one estimated during SAFMED over the North West Mediterranean Sea.

4.4. Comparing the three photochemical metrics: PO_3, OPE, and PRO*x*

We discuss here the consistency of the results derived from the different metrics. We focus on the PO_3 and PRO*x*. Indeed the OPE calculation was not possible either due to the absence of correlation between O_x and NO_z inside the plumes or the absence of NO_y measurement (DACCIWA). The ozone production (PO_3) derived from eqn (7) provides a real-time calculation of the production at the time of measurements while the PRO*x* and OPE provide an integrated photochemical production calculated over the whole plume.

PO_3 is consistent with the Leighton ratio (Φ) calculation. However, PO_3 usually shows an opposite feature to the one of the PRO*x* metrics. While the PRO*x* metric suggests a significant photochemical production of oxidants in the Paris plume (up to 27 ppb per hour for a 100 ppb CO enhancement) except for flight 30, the PO_3 metric points out the absence of photochemical ozone production inside the plume. During DACCIWA, PO_3 is significant inside the plume while $\Delta[O_x]/\Delta[CO]$ is constant with the processing time. In PO_3 calculation, NO is assumed to be at the steady state. When the aircraft crosses the fresh air masses with high NO, the steady state conditions might not be encountered and ozone is titrated by NO. PRO*x* assumes that there is no additional emission of CO or ozone removal along the flight path to be able to quantify oxidant production.

In addition, the effect of the uncertainty of Φ (Section 3.2.2) on PO_3 calculation is examined here. In eqn (7) we replaced the source term $J_{NO2}[NO_2]$ by $\Phi \times k_3[O_3][NO]$ deduced from the Leighton ratio expression (eqn (1)). As a consequence PO_3 equals $(\Phi - 1) \times k_3[O_3][NO]$. Given the uncertainties on the different terms, the relative uncertainty on PO_3 is roughly ±57%. When applying +32% to calculated Φ values for flight 36, we get a slightly positive PO_3 on the plume edges of a few ppb h^{-1} on average which is more consistent with the PRO*x* calculation. One should note that the uncertainty on PRO*x* is lower and does not exceed 30% (Fig. 13) except for flight 25. Our results suggest how the determined uncertainty (σ) on Φ can affect the calculated ozone production derived from the PSS.

5. Conclusion

In this study, we have analyzed different indicators for photochemical ozone formation in contrasting conditions from three summer airborne campaigns, namely MEGAPOLI (2009), ChArMEx/SAFMED (2013), and DACCIWA (2016), respectively performed around Paris, France, over the northwestern Mediterranean basin, and southern West Africa.

After careful identification of polluted plumes within the boundary layer, the analysis of photochemistry is based on

various metrics previously used in the literature, namely the Leighton ratio, the estimation of peroxy radical mixing ratios from the photostationary steady-state method, ozone production rates, the ozone formation potential, and on a new metric defined as the CO-adjusted production rate of oxidants (PRO*x*).

It is found that the Leighton ratio is usually within $1 \pm \sigma$ PSS limits in the plume and deviates positively from unity outside the plume for most of the flights. The deviation of the Leighton ratio from unity is explained by the rapid change of the mixing ratios of ozone and nitrogen oxides, and the photolysis frequency of NO_2, as well as by the presence of other components that convert NO to NO_2, such as peroxy radicals and halogen monoxide. Predicted ozone is well explained by the PSS formula inside the plume when the Leighton ratio is within the PSS range for all the contrasting regions.

While in our analysis the mean $[RO_x]$ mixing ratio barely reaches 29 ppt inside the plume during SAFMED (flight 46), the $[RO_x]$ mixing ratios outside the plumes can reach more than a hundred ppt in SWA and Paris on average. While an overestimation is suspected, those values are consistent with the ones from the literature.

The mean ozone production is higher downwind Paris (30 ppb h^{-1} on average) compared to SWA (20 ppb h^{-1}) and WMB (6 ppb h^{-1}). To investigate the ozone sensitivity towards NO_x and VOC in Paris, WMB, and SWA, O_3 mixing ratios have been plotted against the NO mixing ratio. It is found that Paris and SWA are VOC-sensitive inside the plumes. In the WMB, the picture is not as clear while a NO_x-sensitive regime is expected from previous studies. The ozone production efficiency could be calculated as the slope of the scatterplot of O_x *vs.* NO_z for the MEGAPOLI flights. It is found that values of OPE range between about 5 to 7 with a coefficient of correlation between 0.33 and 0.53. This suggests that Paris is still under a VOC-sensitive regime or in a transition regime outside the plumes according to Sillman[141] since OPE is lower than 7.

Finally, the oxidant production rate PRO*x* has been quantified. Its values vary between 0 and 0.27 $ppb_{[Ox]}\ ppb_{[CO]}^{-1}\ h^{-1}$. PRO*x* is positive in the Paris (4 flights over 6) and WMB plumes whereas it is close to zero in SWA plumes. The consistency between the various metrics is discussed: the determined uncertainty on the Leighton ratio value could affect the differences in the estimation of the photochemical oxidant production by PO_3 and PRO*x*. The presence of vegetation and high humidity levels (deposition sink for ozone) and additional CO emissions along the plume travel during DACCIWA might shapes the PRO*x*. Even limited in number, PRO*x* values from this study set a benchmark for future photochemical studies to compare with: Paris as representative of an anthropogenic continental urban plume and WMB as representative of a biogenic continental plume.

Data availability

All data used in this study are available on the AERIS Data and Service Center. DACCIWA: **https://baobab.sedoo.fr/DACCIWA**. MEGAPOLI: **https://cds-espri.ipsl.upmc.fr/megapoli/index.jsp**. ChArMEX/SAFMED: **https://mistrals.sedoo.fr/ChArMEx/**.

Author contributions

BT: conceptualization, data analysis, paper writing; PD: reviewing, editing, figure design; AC: PhD co-supervision, airborne field data collection during the three campaigns, editing; VM: airborne data collection during MEGAPOLI, editing, reviewing; JFD: editing, reviewing; MB: PI of the MEGAPOLI airborne experiment, interpretation, editing, reviewing; KS: PI of the SAFMED project, editing, reviewing; FD: PI of the ChArMEx project, editing, reviewing; AB: supervision, co-PI of the SAFMED and MEGAPOLI airborne campaigns, conceptualization, writing, reviewing.

Conflicts of interest

There are no conflicts to declare.

Acknowledgements

Airborne data were obtained using the ATR-42 aircraft managed by Safire, the French facility for airborne research, an infrastructure of the French National Center for Scientific Research (CNRS), Météo-France and the French National Center for Space Studies (CNES). Part of the research leading to these results has received funding from the European Union's Seventh Framework Programme FP/2007-2011 within the project MEGAPOLI, grant agreement 212520. The authors also acknowledge for their financial support both the ANR through the MEGAPOLI PARIS project and the INSU/LEFE program through the MEGAPOLI France project. This study also received financial support from MISTRALS by ADEME, CEA, INSU, and Meteo-France and from ANR through the SAFMED project (grant number ANR-12-BS06-0013-2502). Finally, this work has received funding from the European Union Seventh Framework Programme (FP7/2007-2013) under grant agreement number 603502 (EU project DACCIWA: dynamics-aerosol-chemistry-cloud interactions in West Africa). The authors would also like to address a special thanks to the pilots and flight crew from Safire for their enthusiasm and support during the measurement campaigns aboard the ATR 42 aircraft. In addition, the authors are very grateful to Eric Hamonou for his logistical help in organizing the ChArMEx/SAFMED campaign, S. Chevallier, C. Gaimoz, S. Triquet and N. Grand from LISA for their technical support for the implementation of trace gas instrumentation during the MEGAPOLI and SAFMED campaigns.

References

1 B. J. Finlayson-Pitts and J. N. Pitts, *Chemistry of the upper and lower atmosphere: theory, experiments, and applications*, Academic Press, 2000.
2 M. L. Bell, R. D. Peng and F. Dominici, The exposure-response curve for ozone and risk of mortality and the adequacy of current ozone regulations, *Environ. Health Perspect.*, 2006, **114**, 532–536.
3 A. Gryparis, B. Forsberg, K. Katsouyanni, A. Analitis, G. Touloumi, J. Schwartz, E. Samoli, S. Medina, H. R. Anderson, E. M. Niciu, H.-E. Wichmann, B. Kriz,

M. Kosnik, J. Skorkovsky, J. M. Vonk and Z. Dörtbudak, Acute Effects of Ozone on Mortality from the 'Air Pollution and Health: A European Approach' Project, *Am. J. Respir. Crit. Care Med.*, 2004, **170**, 1080–1087.

4 S. V. Krupa and W. J. Manning, Atmospheric ozone: formation and effects on vegetation, *Environ. Pollut.*, 1988, **50**, 101–137.

5 P. B. Reich and R. G. Amundson, Ambient Levels of Ozone Reduce Net Photosynthesis in Tree and Crop Species, *Science*, 1985, **230**, 566–570.

6 E. L. Fiscus, F. L. Booker and K. O. Burkey, *Plant, Cell Environ.*, 2005, **28**, 997–1011.

7 M. R. Ashmore, Assessing the future global impacts of ozone on vegetation, *Plant, Cell Environ.*, 2005, **28**, 949–964.

8 M. G. Schultz, S. Schröder, O. Lyapina, O. R. Cooper, I. Galbally, I. Petropavlovskikh, E. Von Schneidemesser, H. Tanimoto, Y. Elshorbany, M. Naja, R. J. Seguel, U. Dauert, P. Eckhardt, S. Feigenspan, M. Fiebig, A. G. Hjellbrekke, Y. D. Hong, P. C. Kjeld, H. Koide, G. Lear, D. Tarasick, M. Ueno, M. Wallasch, D. Baumgardner, M. T. Chuang, R. Gillett, M. Lee, S. Molloy, R. Moolla, T. Wang, K. Sharps, J. A. Adame, G. Ancellet, F. Apadula, P. Artaxo, M. E. Barlasina, M. Bogucka, P. Bonasoni, L. Chang, A. Colomb, E. Cuevas-Agulló, M. Cupeiro, A. Degorska, A. Ding, M. Fröhlich, M. Frolova, H. Gadhavi, F. Gheusi, S. Gilge, M. Y. Gonzalez, V. Gros, S. H. Hamad, D. Helmig, D. Henriques, O. Hermansen, R. Holla, J. Hueber, U. Im, D. A. Jaffe, N. Komala, D. Kubistin, K. S. Lam, T. Laurila, H. Lee, I. Levy, C. Mazzoleni, L. R. Mazzoleni, A. McClure-Begley, M. Mohamad, M. Murovec, M. Navarro-Comas, F. Nicodim, D. Parrish, K. A. Read, N. Reid, L. Ries, P. Saxena, J. J. Schwab, Y. Scorgie, I. Senik, P. Simmonds, V. Sinha, A. I. Skorokhod, G. Spain, W. Spangl, R. Spoor, S. R. Springston, K. Steer, M. Steinbacher, E. Suharguniyawan, P. Torre, T. Trickl, L. Weili, R. Weller, X. Xiaobin, L. Xue and M. Zhiqiang, Tropospheric Ozone Assessment Report: database and metrics data of global surface ozone observations, *Elementa*, 2017, **5**, 43.

9 A. Gaudel, O. R. Cooper, G. Ancellet, B. Barret, A. Boynard, J. P. Burrows, C. Clerbaux, P.-F. Coheur, J. Cuesta, E. Cuevas, S. Doniki, G. Dufour, F. Ebojie, G. Foret, O. Garcia, M. J. Granados-Muñoz, J. W. Hannigan, F. Hase, B. Hassler, G. Huang, D. Hurtmans, D. Jaffe, N. Jones, P. Kalabokas, B. Kerridge, S. Kulawik, B. Latter, T. Leblanc, E. Le Flochmoën, W. Lin, J. Liu, X. Liu, E. Mahieu, A. McClure-Begley, J. L. Neu, M. Osman, M. Palm, H. Petetin, I. Petropavlovskikh, R. Querel, N. Rahpoe, A. Rozanov, M. G. Schultz, J. Schwab, R. Siddans, D. Smale, M. Steinbacher, H. Tanimoto, D. W. Tarasick, V. Thouret, A. M. Thompson, T. Trickl, E. Weatherhead, C. Wespes, H. M. Worden, C. Vigouroux, X. Xu, G. Zeng and J. Ziemke, Tropospheric Ozone Assessment Report: present-day distribution and trends of tropospheric ozone relevant to climate and global atmospheric chemistry model evaluation, *Elementa*, 2018, **6**, 39.

10 W. L. Chameides, F. Fehsenfeld, M. O. Rodgers, C. Cardelino, J. Martinez, D. Parrish, W. Lonneman, D. R. Lawson, R. A. Rasmussen, P. Zimmerman, J. Greenberg, P. Mlddleton and T. Wang, Ozone precursor relationships in the ambient atmosphere, *J. Geophys. Res.*, 1992, **97**, 6037.

11 F. M. Bowman and J. H. Seinfeld, Ozone productivity of atmospheric organics, *J. Geophys. Res.*, 1994, **99**, 5309.

12 B. J. Finlayson-Pitts and J. N. Pitts, Tropospheric air pollution: ozone, airborne toxics, polycyclic aromatic hydrocarbons, and particles, *Science*, 1997, **276**, 1045–1052.

13 X. Tang, Z. Wang, J. Zhu, A. E. Gbaguidi, Q. Wu, J. Li and T. Zhu, Sensitivity of ozone to precursor emissions in urban Beijing with a Monte Carlo scheme, *Atmos. Environ.*, 2010, **44**, 3833–3842.

14 M. J. Molina and L. T. Molina, Megacities and atmospheric pollution, *J. Air Waste Manage. Assoc.*, 2004, **54**, 644–680.

15 L. Ran, C. Zhao, F. Geng, X. Tie, X. Tang, L. Peng, G. Zhou, Q. Yu, J. Xu and A. Guenther, Ozone photochemical production in urban Shanghai, China: analysis based on ground level observations, *J. Geophys. Res.*, 2009, **114**, D15301.

16 C. K. Chan and X. Yao, Air pollution in mega cities in China, *Atmos. Environ.*, 2008, **42**, 1–42.

17 M. Shao, X. Tang, Y. Zhang and W. Li, City clusters in China: air and surface water pollution, *Front. Ecol. Environ.*, 2006, **4**, 353–361.

18 S. Sillman and D. He, Some theoretical results concerning O_3-NO_x-VOC chemistry and NO_x-VOC indicators, *J. Geophys. Res.: Atmos.*, 2002, **107**, ACH 26.

19 M. J. Newland, D. J. Bryant, R. E. Dunmore, T. J. Bannan, W. J. F. Acton, B. Langford, J. R. Hopkins, F. A. Squires, W. Dixon, W. S. Drysdale, P. D. Ivatt, M. J. Evans, P. M. Edwards, L. K. Whalley, D. E. Heard, E. J. Slater, R. Woodward-Massey, C. Ye, A. Mehra, S. D. Worrall, A. Bacak, H. Coe, C. J. Percival, C. N. Hewitt, J. D. Lee, T. Cui, J. D. Surratt, X. Wang, A. C. Lewis, A. R. Rickard and J. F. Hamilton, Low-NO atmospheric oxidation pathways in a polluted megacity, *Atmos. Chem. Phys.*, 2021, **21**, 1613–1625.

20 W. Chameides, R. W. Lindsay, J. Richardson and C. S. Kiang, The role of biogenic hydrocarbons in urban photochemical smog: Atlanta as a case study, *Science*, 1988, **241**, 1473–1475.

21 C. Calfapietra, S. Fares, F. Manes, A. Morani, G. Sgrigna and F. Loreto, Role of Biogenic Volatile Organic Compounds (BVOC) emitted by urban trees on ozone concentration in cities: a review, *Environ. Pollut.*, 2013, **183**, 71–80.

22 A. Lefohn, D. Shadwick and S. J. Oltmans, Environment and undefined 2010, characterizing changes in surface ozone levels in metropolitan and rural areas in the United States for 1980–2008 and 1994–2008, *Atmos. Environ.*, 2010, **44**(39), 5199–5210.

23 O. R. Cooper, R. S. Gao, D. Tarasick, T. Leblanc and C. Sweeney, Long-term ozone trends at rural ozone monitoring sites across the United States, 1990-2010, *J.*

Geophys. Res.: Atmos., 2012, **117**, 22, DOI: **10.1029/2012JD018261**.

24 H. Simon, A. Reff, B. Wells, J. Xing and N. Frank, Ozone Trends across the United States over a Period of Decreasing NO_x and VOC Emissions, *Environ. Sci. Technol.*, 2015, **49**, 186–195.

25 M. Lin, L. W. Horowitz, R. Payton, A. M. Fiore and G. Tonnesen, US surface ozone trends and extremes from 1980 to 2014: quantifying the roles of rising Asian emissions, domestic controls, wildfires, and climate, *Atmos. Chem. Phys.*, 2017, **17**, 2943–2970.

26 P. J. Young, V. Naik, A. M. Fiore, A. Gaudel, J. Guo, M. Y. Lin, J. L. Neu, D. D. Parrish, H. E. Rieder, J. L. Schnell, S. Tilmes, O. Wild, L. Zhang, J. Ziemke, J. Brandt, A. Delcloo, R. M. Doherty, C. Geels, M. I. Hegglin, L. Hu, U. Im, R. Kumar, A. Luhar, L. Murray, D. Plummer, J. Rodriguez, A. Saiz-Lopez, M. G. Schultz, M. T. Woodhouse and G. Zeng, Tropospheric Ozone Assessment Report: assessment of global-scale model performance for global and regional ozone distributions, variability, and trends, *Elementa*, 2018, **6**, DOI: **10.1525/elementa.265**.

27 R. G. Derwent, M. E. Jenkin, M. J. Pilling, W. P. L. Carter and A. Kaduwela, Reactivity Scales as Comparative Tools for Chemical Mechanisms, *J. Air Waste Manage. Assoc.*, 2010, **60**, 914–924.

28 Air quality in Europe – 2016 report – European Environment Agency.

29 M. Andre, K. Sartelet, S. Moukhtar, J. M. Andre and M. Redaelli, Diesel, petrol or electric vehicles: what choices to improve urban air quality in the Ile-de-France region? A simulation platform and case study, *Atmos. Environ.*, 2020, **241**, 117752.

30 N. A. Krotkov, C. A. McLinden, C. Li, L. N. Lamsal, E. A. Celarier, S. V. Marchenko, W. H. Swartz, E. J. Bucsela, J. Joiner, B. N. Duncan, K. F. Boersma, J. P. Veefkind, P. F. Levelt, V. E. Fioletov, R. R. Dickerson, H. He, Z. Lu and D. G. Streets, Aura OMI observations of regional SO_2 and NO_2 pollution changes from 2005 to 2015, *Atmos. Chem. Phys.*, 2016, **16**, 4605–4629.

31 F. Liu, Q. Zhang, R. J. Van Der A, B. Zheng, D. Tong, L. Yan, Y. Zheng and K. He, Recent reduction in NO_x emissions over China: synthesis of satellite observations and emission inventories, *Environ. Res. Lett.*, 2016, **11**, 114002.

32 T. Wang, A. Ding, J. Gao and W. S. Wu, Strong ozone production in urban plumes from Beijing, China, *Geophys. Res. Lett.*, 2006, **21**, DOI: **10.1029/2006GL027689**.

33 Z. Ma, J. Xu, W. Quan, Z. Zhang, W. Lin and X. Xu, Significant increase of surface ozone at a rural site, north of eastern China, *Atmos. Chem. Phys.*, 2016, **16**, 3969–3977.

34 W. Xu, W. Lin, X. Xu, J. Tang, J. Huang, H. Wu and X. Zhang, Long-term trends of surface ozone and its influencing factors at the Mt Waliguan GAW station, China – part 1: overall trends and characteristics, *Atmos. Chem. Phys.*, 2016, **16**, 6191–6205.

35 B. Zhao, S. X. Wang, H. Liu, J. Y. Xu, K. Fu, Z. Klimont, J. M. Hao, K. B. He, J. Cofala and M. Amann, NO_x emissions in China: historical trends and future perspectives, *Atmos. Chem. Phys.*, 2013, **13**, 9869–9897.

36 K.-L. Chang, I. Petropavlovskikh, O. R. Cooper, M. G. Schultz and T. Wang, Regional trend analysis of surface ozone observations from monitoring networks in eastern North America, Europe and East Asia, *Elementa*, 2017, **5**, DOI: **10.1525/elementa.243**.

37 S. C. Liu, M. Trainer, F. C. Fehsenfeld, D. D. Parrish, E. J. Williams, D. W. Fahey, G. Hübler and P. C. Murphy, Ozone production in the rural troposphere and the implications for regional and global ozone distributions, *J. Geophys. Res.*, 1987, **92**, 4191.

38 Z. L. Fleming, R. M. Doherty, E. Von Schneidemesser, C. S. Malley, O. R. Cooper, J. P. Pinto, A. Colette, X. Xu, D. Simpson, M. G. Schultz, A. S. Lefohn, S. Hamad, R. Moolla, S. Solberg and Z. Feng, Tropospheric Ozone Assessment Report: present-day ozone distribution and trends relevant to human health, *Elementa*, 2018, **6**, DOI: **10.1525/elementa.273**.

39 A. S. Lefohn, C. S. Malley, L. Smith, B. Wells, M. Hazucha, H. Simon, V. Naik, G. Mills, M. G. Schultz, E. Paoletti, A. De Marco, X. Xu, L. Zhang, T. Wang, H. S. Neufeld, R. C. Musselman, D. Tarasick, M. Brauer, Z. Feng, H. Tang, K. Kobayashi, P. Sicard, S. Solberg and G. Gerosa, Tropospheric Ozone Assessment Report: global ozone metrics for climate change, human health, and crop/ecosystem research, *Elementa*, 2018, **6**, DOI: **10.1525/elementa.279**.

40 G. Mills, H. Pleijel, C. S. Malley, B. Sinha, O. R. Cooper, M. G. Schultz, H. S. Neufeld, D. Simpson, K. Sharps, Z. Feng, G. Gerosa, H. Harmens, K. Kobayashi, P. Saxena, E. Paoletti, V. Sinha and X. Xu, Tropospheric Ozone Assessment Report: present-day tropospheric ozone distribution and trends relevant to vegetation, *Elementa*, 2018, **6**, DOI: **10.1525/elementa.302**.

41 D. Tarasick, I. E. Galbally, O. R. Cooper, M. G. Schultz, G. Ancellet, T. Leblanc, T. J. Wallington, J. Ziemke, X. Liu, M. Steinbacher, J. Staehelin, C. Vigouroux, J. W. Hannigan, O. García, G. Foret, P. Zanis, E. Weatherhead, I. Petropavlovskikh, H. Worden, M. Osman, J. Liu, K.-L. Chang, A. Gaudel, M. Lin, M. Granados-Muñoz, A. M. Thompson, S. J. Oltmans, J. Cuesta, G. Dufour, V. Thouret, B. Hassler, T. Trickl and J. L. Neu, Tropospheric Ozone Assessment Report: tropospheric ozone from 1877 to 2016, observed levels, trends and uncertainties, *Elementa*, 2019, **7**, 39.

42 X. Xu, W. Lin, W. Xu, J. Jin, Y. Wang, G. Zhang, X. Zhang, Z. Ma, Y. Dong, Q. Ma, D. Yu, Z. Li, D. Wang and H. Zhao, Long-term changes of regional ozone in China: implications for human health and ecosystem impacts, *Elementa*, **2020**, DOI: **10.1525/elementa.409**.

43 A. Baklanov, M. Lawrence, S. Pandis, A. Mahura, S. Finardi, N. Moussiopoulos, M. Beekmann, P. Laj, L. Gomes, J.-L. Jaffrezo, A. Borbon, I. Coll, V. Gros, J. Sciare, J. Kukkonen, S. Galmarini, F. Giorgi, S. Grimmond, I. Esau, A. Stohl, B. Denby, T. Wagner, T. Butler, U. Baltensperger, P. Builtjes, D. van den Hout, H. D. van

der Gon, B. Collins, H. Schluenzen, M. Kulmala, S. Zilitinkevich, R. Sokhi, R. Friedrich, J. Theloke, U. Kummer, L. Jalkinen, T. Halenka, A. Wiedensholer, J. Pyle and W. B. Rossow, MEGAPOLI: concept of multi-scale modelling of megacity impact on air quality and climate, *Adv. Sci. Res.*, 2010, **4**, 115–120.

44 F. Dulac, in *EGU General Assembly*, 2014, vol. 16, p. 11441.

45 P. Knippertz, A. H. Fink, A. Deroubaix, E. Morris, F. Tocquer, M. J. Evans, C. Flamant, M. Gaetani, C. Lavaysse, C. Mari, J. H. Marsham, R. Meynadier, A. Affo-Dogo, T. Bahaga, F. Brosse, K. Deetz, R. Guebsi, I. Latifou, M. Maranan, P. D. Rosenberg and A. Schlueter, A meteorological and chemical overview of the DACCIWA field campaign in West Africa in June-July 2016, *Atmos. Chem. Phys.*, 2017, **17**, 10893–10918.

46 E. Freney, K. Sellegri, M. Chrit, K. Adachi, J. Brito, A. Waked, A. Borbon, A. Colomb, R. Dupuy, J. M. Pichon, L. Bouvier, C. Delon, C. Jambert, P. Durand, T. Bourianne, C. Gaimoz, S. Triquet, A. Féron, M. Beekmann, F. Dulac and K. Sartelet, Aerosol composition and the contribution of SOA formation over Mediterranean forests, *Atmos. Chem. Phys.*, 2018, **18**, 7041–7056.

47 P. S. Monks, C. Granier, S. Fuzzi, A. Stohl, M. L. Williams, H. Akimoto, M. Amann, A. Baklanov, U. Baltensperger, I. Bey, N. Blake, R. S. Blake, K. Carslaw, O. R. Cooper, F. Dentener, D. Fowler, E. Fragkou, G. J. Frost, S. Generoso, P. Ginoux, V. Grewe, A. Guenther, H. C. Hansson, S. Henne, J. Hjorth, A. Hofzumahaus, H. Huntrieser, I. S. A. Isaksen, M. E. Jenkin, J. Kaiser, M. Kanakidou, Z. Klimont, M. Kulmala, P. Laj, M. G. Lawrence, J. D. Lee, C. Liousse, M. Maione, G. McFiggans, A. Metzger, A. Mieville, N. Moussiopoulos, J. J. Orlando, C. D. O'Dowd, P. I. Palmer, D. D. Parrish, A. Petzold, U. Platt, U. Pöschl, A. S. H. Prévôt, C. E. Reeves, S. Reimann, Y. Rudich, K. Sellegri, R. Steinbrecher, D. Simpson, H. ten Brink, J. Theloke, G. R. van der Werf, R. Vautard, V. Vestreng, C. Vlachokostas and R. von Glasow, Atmospheric composition change – global and regional air quality, *Atmos. Environ.*, 2009, **43**, 5268–5350.

48 J. Lelieveld, P. Hadjinicolaou, E. Kostopoulou, J. Chenoweth, M. El Maayar, C. Giannakopoulos, C. Hannides, M. A. Lange, M. Tanarhte, E. Tyrlis and E. Xoplaki, Climate change and impacts in the Eastern Mediterranean and the Middle East, *Clim. Change*, 2012, **114**, 667–687.

49 C. Flamant, A. Deroubaix, P. Chazette, J. Brito, M. Gaetani, P. Knippertz, A. H. Fink, G. de Coetlogon, L. Menut, A. Colomb, C. Denjean, R. Meynadier, P. Rosenberg, R. Dupuy, P. Dominutti, J. Duplissy, T. Bourrianne, A. Schwarzenboeck, M. Ramonet and J. Totems, Aerosol distribution in the northern Gulf of Guinea: local anthropogenic sources, long-range transport, and the role of coastal shallow circulations, *Atmos. Chem. Phys.*, 2018, **18**, 12363–12389.

50 E. C. Wood, S. C. Herndon, T. B. Onasch, J. H. Kroll, M. R. Canagaratna, C. E. Kolb, D. R. Worsnop, J. A. Neuman, R. Seila, M. Zavala and W. B. Knighton, A case study of ozone production, nitrogen oxides, and the radical budget in Mexico City, *Atmos. Chem. Phys.*, 2009, **9**, 2499–2516.

51 J. A. Thornton, P. J. Wooldridge, R. C. Cohen, M. Martinez, H. Harder, W. H. Brune, E. J. Williams, J. M. Roberts, F. C. Fehsenfeld, S. R. Hall, R. E. Shetter, B. P. Wert and A. Fried, Ozone production rates as a function of NO_x abundances and HO_x production rates in the Nashville urban plume, *J. Geophys. Res.*, 2002, **107**, 1–17.

52 G. M. Mazzuca, X. Ren, C. P. Loughner, M. Estes, J. H. Crawford, K. E. Pickering, A. J. Weinheimer and R. R. Dickerson, Ozone production and its sensitivity to NO_x and VOCs: results from the DISCOVER-AQ field experiment, Houston 2013, *Atmos. Chem. Phys.*, 2016, **16**, 14463–14474.

53 H. Guo, K. Chen, P. Wang, J. Hu, Q. Ying, A. Gao and H. Zhang, Simulation of summer ozone and its sensitivity to emission changes in China, *Atmos. Pollut. Res.*, 2019, **10**, 1543–1552.

54 Z. Tan, K. Lu, M. Jiang, R. Su, H. Dong, L. Zeng, S. Xie, Q. Tan and Y. Zhang, Exploring ozone pollution in Chengdu, southwestern China: a case study from radical chemistry to O_3-VOC-NO_x sensitivity, *Sci. Total Environ.*, 2018, **636**, 775–786.

55 B. A. Ridley, S. Madronich, R. B. Chatfield, J. G. Walega, R. E. Shetter, M. A. Carroll and D. D. Montzka, Measurements and model simulations of the photostationary state during the Mauna Loa Observatory Photochemistry Experiment: implications for radical concentrations and ozone production and loss rates, *J. Geophys. Res.*, 1992, **97**, 10375.

56 A. Volz-Thomas, Inorganic trace gases and peroxy radicals during BERLIOZ at Pabstthum: an investigation of the photostationary state of NO_x and O_3, *J. Geophys. Res.*, 2003, **108**, 8248.

57 K. Mannschreck, S. Gilge, C. Plass-Duelmer, W. Fricke and H. Berresheim, Assessment of the NO-NO_2-O_3 photostationary state applicability on long-term measurements at the GAW global station Hohenpeissenberg, Germany, *Atmos. Chem. Phys. Discuss.*, 2004, **4**, 2003–2036.

58 R. J. Griffin, P. J. Beckman, R. W. Talbot, B. C. Sive and R. K. Varner, Deviations from ozone photostationary state during the International Consortium for Atmospheric Research on Transport and Transformation 2004 campaign: use of measurements and photochemical modeling to assess potential causes, *J. Geophys. Res.: Atmos.*, 2007, **112**, 1–16.

59 J. Yang, Photostationary state deviation–estimated peroxy radicals and their implications for HO_x and ozone photochemistry at a remote northern Atlantic coastal site, *J. Geophys. Res.*, 2004, **109**, D02312.

60 J. Matsumoto, N. Kosugi, A. Nishiyama, R. Isozaki, Y. Sadanaga, S. Kato, H. Bandow and Y. Kajii, Examination on photostationary state of NO_x in the urban atmosphere in Japan, *Atmos. Environ.*, 2006, **40**, 3230–3239.

61 R. A. Zaveri, C. M. Berkowitz, L. I. Kleinman, S. R. Springston, P. V. Doskey, W. A. Lonneman and C. W. Spicer, Ozone production efficiency and NO_x depletion in an urban plume: interpretation of field observations and implications for evaluating O_3-NO_x-VOC sensitivity, *J. Geophys. Res.: Atmos.*, 2003, **108**, 4436.

62 Y. F. Elshorbany, J. Kleffmann, R. Kurtenbach, M. Rubio, E. Lissi, G. Villena, E. Gramsch, A. R. Rickard, M. J. Pilling and P. Wiesen, Summertime photochemical ozone formation in Santiago, Chile, *Atmos. Environ.*, 2009, **43**, 6398–6407.

63 N. Cheng, Z. Chen, F. Sun, R. Sun, X. Dong, X. Xie and C. Xu, Ground ozone concentrations over Beijing from 2004 to 2015: variation patterns, indicative precursors and effects of emission-reduction, *Environ. Pollut.*, 2018, **237**, 262–274.

64 L. Hembeck, H. He, T. P. Vinciguerra, T. P. Canty, R. R. Dickerson, R. J. Salawitch and C. Loughner, Measured and modelled ozone photochemical production in the Baltimore-Washington airshed, *Atmos. Environ.: X*, 2019, **2**, 100017.

65 A. Baklanov, M. Lawrence, S. Pandis, A. Mahura, S. Finardi, N. Moussiopoulos, M. Beekmann, P. Laj, L. Gomes, J.-L. Jaffrezo, A. Borbon, I. Coll, V. Gros, J. Sciare, J. Kukkonen, S. Galmarini, F. Giorgi, S. Grimmond, I. Esau, A. Stohl, B. Denby, T. Wagner, T. Butler, U. Baltensperger, P. Builtjes, D. van den Hout, H. D. van der Gon, B. Collins, H. Schluenzen, M. Kulmala, S. Zilitinkevich, R. Sokhi, R. Friedrich, J. Theloke, U. Kummer, L. Jalkinen, T. Halenka, A. Wiedensholer, J. Pyle and W. B. Rossow, MEGAPOLI: concept of multi-scale modelling of megacity impact on air quality and climate, *Adv. Sci. Res.*, 2010, **4**, 115–120.

66 A. Borbon, J. B. Gilman, W. C. Kuster, N. Grand, S. Chevaillier, A. Colomb, C. Dolgorouky, V. Gros, M. Lopez, R. Sarda-Esteve, J. Holloway, J. Stutz, H. Petetin, S. McKeen, M. Beekmann, C. Warneke, D. D. Parrish and J. A. de Gouw, Emission ratios of anthropogenic volatile organic compounds in northern mid-latitude megacities: observations versus emission inventories in Los Angeles and Paris, *J. Geophys. Res.: Atmos.*, 2013, **118**, 2041–2057.

67 E. J. Freney, K. Sellegri, F. Canonaco, A. Colomb, A. Borbon, V. Michoud, S. Crumeyrolle, N. Amarouche, T. Bourianne, L. Gomes, A. S. H. Prevot, M. Beekmann and A. Schwarzenböeck, Characterizing the impact of urban emissions on regional aerosol particles: airborne measurements during the MEGAPOLI experiment, *Atmos. Chem. Phys.*, 2014, **14**, 1397–1412.

68 Q. J. Zhang, M. Beekmann, E. Freney, K. Sellegri, J. M. Pichon, A. Schwarzenboeck, A. Colomb, T. Bourrianne, V. Michoud and A. Borbon, Formation of secondary organic aerosol in the Paris pollution plume and its impact on surrounding regions, *Atmos. Chem. Phys.*, 2015, **15**, 13973–13992.

69 P. Knippertz, M. J. Evans, P. R. Field, A. H. Fink, C. Liousse and J. H. Marsham, The possible role of local air pollution in climate change in West Africa, *Nat. Clim. Change*, 2015, **5**, 815–822.

70 J. Brito, E. Freney, P. Dominutti, A. Borbon, S. L. Haslett, A. M. Batenburg, A. Colomb, R. Dupuy, C. Denjean, F. Burnet, T. Bourriane, A. Deroubaix, K. Sellegri, S. Borrmann, H. Coe, C. Flamant, P. Knippertz and A. Schwarzenboeck, Assessing the role of anthropogenic and biogenic sources on PM_1 over southern West Africa using aircraft measurements, *Atmos. Chem. Phys.*, 2018, **18**, 757–772.

71 P. Nedelec, J.-P. Cammas, V. Thouret, G. Athier, J.-M. Cousin, C. Legrand, C. Abonnel, F. Lecoeur, G. Cayez and C. Marizy, An improved infrared carbon monoxide analyser for routine measurements aboard commercial Airbus aircraft: technical validation and first scientific results of the MOZAIC III programme, *Atmos. Chem. Phys.*, 2003, **3**, 1551–1564.

72 V. Thouret, A. Marenco, P. Sabatier, J. A. Logan, P. Ndec and C. Grouhel, Comparisons of ozone measurements from the MOZAIC airborne program and the ozone sounding network at eight locations G, *J. Geophys. Res.*, 1998, 25695–25720.

73 R. Blot, P. Nedelec, D. Boulanger, P. Wolff, B. Sauvage, J.-M. Cousin, G. Athier, A. Zahn, F. Obersteiner, D. Scharffe, H. Petetin, Y. Bennouna, H. Clark and V. Thouret, Internal consistency of the IAGOS ozone and carbon monoxide measurements for the last 25 years, *Atmos. Meas. Tech.*, 2021, **14**, 3935–3951.

74 A. Filges, C. Gerbig, H. Chen, H. Franke, C. Klaus and A. Jordan, The IAGOS-core greenhouse gas package: a measurement system for continuous airborne observations of CO_2, CH_4, H_2O and CO, *Tellus B*, 2015, **67**, 27989.

75 B. Bohn and H. Zilken, Model-aided radiometric determination of photolysis frequencies in a sunlit atmosphere simulation chamber, *Atmos. Chem. Phys.*, 2005, **5**, 191–206.

76 J. Bechara, A. Borbon, C. Jambert, A. Colomb and P. E. Perros, Evidence of the impact of deep convection on reactive volatile organic compounds in the upper tropical troposphere during the AMMA experiment in West Africa, *Atmos. Chem. Phys.*, 2010, **10**, 10321–10334.

77 J. Bechara, A. Borbon, C. Jambert, A. Colomb and P. E. Perros, Evidence of the impact of deep convection on reactive volatile organic compounds in the upper tropical troposphere during the AMMA experiment in West Africa, *Atmos. Chem. Phys.*, 2010, **10**, 10321–10334.

78 F. Klein, S. M. Pieber, H. Ni, G. Stefenelli, A. Bertrand, D. Kilic, V. Pospisilova, B. Temime-Roussel, N. Marchand, I. El Haddad, J. G. Slowik, U. Baltensperger, J. Cao, R. Huang and A. S. H. Prévôt, Characterization of Gas-Phase Organics Using Proton Transfer Reaction Time-of-Flight Mass Spectrometry: Residential Coal Combustion, *Environ. Sci. Technol.*, 2018, **52**, 2612–2617.

79 M. Haeffelin, L. Barthès, O. Bock, C. Boitel, S. Bony, D. Bouniol, H. Chepfer, M. Chiriaco, J. Cuesta, J. Delanoë, P. Drobinski, J.-L. Dufresne, C. Flamant, M. Grall, A. Hodzic, F. Hourdin, F. Lapouge, Y. Lemaître, A. Mathieu, Y. Morille, C. Naud, V. Noël, W. O'Hirok,

J. Pelon, C. Pietras, A. Protat, B. Romand, G. Scialom and R. Vautard, SIRTA, a ground-based atmospheric observatory for cloud and aerosol research, *Ann. Geophys.*, 2005, **23**, 253–275.

80 W. Ait-Helal, A. Borbon, S. Sauvage, J. A. de Gouw, A. Colomb, V. Gros, F. Freutel, M. Crippa, C. Afif, U. Baltensperger, M. Beekmann, J.-F. Doussin, R. Durand-Jolibois, I. Fronval, N. Grand, T. Leonardis, M. Lopez, V. Michoud, K. Miet, S. Perrier, A. S. H. Prévôt, J. Schneider, G. Siour, P. Zapf and N. Locoge, Volatile and intermediate volatility organic compounds in suburban Paris: variability, origin and importance for SOA formation, *Atmos. Chem. Phys.*, 2014, **14**, 10439–10464.

81 C. Di Biagio, L. Doppler, C. Gaimoz, N. Grand, G. Ancellet, J. C. Raut, M. Beekmann, A. Borbon, K. Sartelet, J. L. Attié, F. Ravetta and P. Formenti, Continental pollution in the western Mediterranean basin: vertical profiles of aerosol and trace gases measured over the sea during TRAQA 2012 and SAFMED 2013, *Atmos. Chem. Phys.*, 2015, **15**, 9611–9630.

82 C. Denjean, T. Bourrianne, F. Burnet, M. Mallet, N. Maury, A. Colomb, P. Dominutti, J. Brito, R. Dupuy, K. Sellegri, A. Schwarzenboeck, C. Flamant and P. Knippertz, Overview of aerosol optical properties over southern West Africa from DACCIWA aircraft measurements, *Atmos. Chem. Phys.*, 2020, **20**, 4735–4756.

83 A. F. Stein, R. R. Draxler, G. D. Rolph, B. J. B. Stunder, M. D. Cohen and F. Ngan, *Bull. Am. Meteorol. Soc.*, 2015, **96**, 2059–2077.

84 A. Volz-Thomas, H. Pätz, N. Houben, S. Konrad, D. Mihelcic, T. Klüpfel and D. Perner, Inorganic trace gases and peroxy radicals during BERLIOZ at Pabstthum: an investigation of the photostationary state of NO_x and O_3, *J. Geophys. Res.*, 2003, **108**, 8248.

85 I. Trebs, O. L. Mayol-Bracero, T. Pauliquevis, U. Kuhn, R. Sander, L. Ganzeveld, F. X. Meixner, J. Kesselmeier, P. Artaxo and M. O. Andreae, Impact of the Manaus urban plume on trace gas mixing ratios near the surface in the Amazon basin: implications for the NO-NO_2-O_3 photostationary state and peroxy radical levels, *J. Geophys. Res.: Atmos.*, 2012, **117**, 1–16.

86 M. A. K. Khalil, Steady states and transport processes in urban ozone balances, *npj Clim. Atmos. Sci.*, 2018, **1**, 22.

87 P. Leighton, *Photochemistry of Air Pollution*, Academic Press, 1st edn, 1961.

88 J. H. Seinfeld and S. N. Pandis, *Atmospheric chemistry and physics: from air pollution to climate change*, 1998.

89 D. M. Chate, S. D. Ghude, G. Beig, A. S. Mahajan, C. Jena, R. Srinivas, A. Dahiya and N. Kumar, Deviations from the O_3-NO-NO_2 photo-stationary state in Delhi, India, *Atmos. Environ.*, 2014, **96**, 353–358.

90 C. A. Cantrell, J. G. Calvert, D. D. Parrish, F. C. Fehsenfeld, P. D. Goldan, W. Kuster, E. J. Williams, H. H. Westberg, G. Allwine and R. Martin, Peroxy Radicals as Measured in ROSE and Estimated from Photostationary State Deviations, *J. Geophys. Res.*, 1993, **92**, 18355–18366.

91 D. A. Hauglustaine, S. Madronich, B. A. Ridley, J. G. Walega, C. A. Cantrell, R. E. Shetter and G. Hübler, Observed and model-calculated photostationary state at Mauna Loa Observatory during MLOPEX 2, *J. Geophys. Res.: Atmos.*, 1999, **104**(D23), 30275–30307.

92 Y. Ma, K. Lu, C. C. K. Chou, X. Li and Y. Zhang, Strong deviations from the NO-NO_2-O_3 photostationary state in the Pearl River Delta: indications of active peroxy radical and chlorine radical chemistry, *Atmos. Environ.*, 2017, **163**, 22–34.

93 J. Yang, Photostationary state deviation–estimated peroxy radicals and their implications for HO_x and ozone photochemistry at a remote northern Atlantic coastal site, *J. Geophys. Res.*, 2004, **109**, D02312.

94 J. H. Seinfeld and S. N. Pandis, *Atmospheric Chemistry and Physics. From Air Pollution to Climate Change*, John Wiley & Sons, 2nd edn, 2006.

95 R. Atkinson and A. C. Lloyd, Evaluation of Kinetic and Mechanistic Data for Modeling of Photochemical Smog, *J. Phys. Chem. Ref. Data*, 1984, **13**, 315–444.

96 K. Mannschreck, S. Gilge, C. Plass-Duelmer, W. Fricke and H. Berresheim, Assessment of the applicability of NO-NO_2-O_3 photostationary state to long-term measurements at the Hohenpeissenberg GAW Station, Germany, *Atmos. Chem. Phys.*, 2004, **4**, 1265–1277.

97 R. Atkinson, D. L. Baulch, R. A. Cox, J. N. Crowley, R. F. Hampson, R. G. Hynes, M. E. Jenkin, M. J. Rossi and J. Troe, Evaluated kinetic and photochemical data for atmospheric chemistry: volume I – gas phase reactions of O_x, HO_x, NO_x and SO_x species, *Atmos. Chem. Phys.*, 2004, **4**, 1461–1738.

98 W. L. Chameides and D. D. Davis, Iodine: its possible role in tropospheric photochemistry, *J. Geophys. Res.: Oceans*, 1980, **85**, 7383–7398.

99 S. Madronich and J. G. Calvert, *The NCAR Master Mechanism of the Gas Phase Chemistry - Version 2.0, No. NCAR/TN-333+STR*, University Corporation for Atmospheric Research, Boulder, Colorado, 1989, DOI: DOI: **10.5065/D6HD7SKH**.

100 R. Wayne, I. Barnes, P. Biggs, J. Burrows, C. Canosa-Mas, J. Hjorth, G. Le Bras, G. Moortgat, D. Perner, G. Poulet, G. Restelli and H. Sidebottom, The nitrate radical: physics, chemistry, and the atmosphere, *Atmos. Environ., Part A*, 1991, **25**, 1–203.

101 R. Atkinson, D. L. Baulch, R. A. Cox, R. F. Hampson, J. A. Kerr, M. J. Rossi and J. Troe, Evaluated Kinetic and Photochemical Data for Atmospheric Chemistry: Supplement VI. IUPAC Subcommittee on Gas Kinetic Data Evaluation for Atmospheric Chemistry, *J. Phys. Chem. Ref. Data*, 1997, **26**, 1329–1499.

102 D. D. Parrish, M. Trainer, E. J. Williams, D. W. Fahey, G. Hübler, C. S. Eubank, S. C. Liu, P. C. Murphy, D. L. Albritton and F. C. Fehsenfeld, Measurements of the NO_x-O_3 photostationary state at Niwot Ridge, Colorado, *J. Geophys. Res.*, 1986, **91**, 5361.

103 C. A. Cantrell, R. E. Shetter, J. G. Calvert, F. L. Eisele, E. Williams, K. Baumann, W. H. Brune, P. S. Stevens and

J. H. Mather, Peroxy radicals from photostationary state deviations and steady state calculations during the Tropospheric OH Photochemistry Experiment at Idaho Hill, Colorado, 1993, *J. Geophys. Res.: Atmos.*, 1997, **102**, 6369–6378.

104 L. I. Kleinman, P. H. Daum, Y. N. Lee, L. J. Nunnermácker, S. R. Springston, J. Weinstein-Lloyd and J. Rudolph, Ozone production efficiency in an urban area, *J. Geophys. Res.: Atmos.*, 2002, **107**(23), DOI: 10.1029/2002JD002529.

105 M. Trainer, Correlation of ozone with NO_y in photochemically aged air, *J. Geophys. Res.*, 1993, **98**, 2917–2925.

106 K. J. Olszyna, E. M. Bailey, R. Simonaitis and J. F. Meagher, O_3 and NO_y relationships at a rural site, *J. Geophys. Res.*, 1994, **99**, 14557–1456.

107 L. Kleinman, Y.-N. Lee, S. R. Springston, L. Nunnermacker, X. Zhou, R. Brown, K. Hallock, P. Klotz, D. Leahy, J. H. Lee and L. Newman, Ozone formation at a rural site in the southeastern United States, *J. Geophys. Res.*, 1994, **99**, 3469.

108 L. J. Nunnermacker, D. Imre, P. H. Daum, L. Kleinman, Y.-N. Lee, J. H. Lee, S. R. Springston, L. Newman, J. Weinstein-Lloyd, W. T. Luke, R. Banta, R. Alvarez, C. Senff, S. Sillman, M. Holdren, G. W. Keigley and X. Zhou, Characterization of the Nashville urban plume on July 3 and July 18, 1995, *J. Geophys. Res.: Atmos.*, 1998, **103**, 28129–28148.

109 J. C. S. John, W. L. Chameides and R. Saylor, Role of anthropogenic NO_x and VOC as ozone precursors: a case study from the SOS Nashville/Middle Tennessee Ozone Study, *J. Geophys. Res.: Atmos.*, 1998, **103**, 22415–22423.

110 L. Kleinman, Ozone process insights from field experiments – part II: observation-based analysis for ozone production, *Atmos. Environ.*, 2000, **34**, 2023–2033.

111 H. U. Price, D. A. Jaffe, O. R. Cooper and P. V. Doskey, Photochemistry, ozone production, and dilution during long-range transport episodes from Eurasia to the northwest United States, *J. Geophys. Res.: Atmos.*, 2004, **109**, 1–10.

112 J. Cuesta, Y. Kanaya, M. Takigawa, G. Dufour, M. Eremenko, G. Foret, K. Miyazaki and M. Beekmann, Transboundary ozone pollution across East Asia: daily evolution and photochemical production analysed by IASI + GOME2 multispectral satellite observations and models, *Atmos. Chem. Phys.*, 2018, **18**, 9499–9525.

113 S. C. Liu, Possible effects on tropospheric O_3 and OH due to NO emissions, *Geophys. Res. Lett.*, 1977, **4**(8), DOI: 10.1029/GL004i008p00325.

114 S. C. Herndon, T. B. Onasch, E. C. Wood, J. H. Kroll, M. R. Canagaratna, J. T. Jayne, M. A. Zavala, W. B. Knighton, C. Mazzoleni, M. K. Dubey, I. M. Ulbrich, J. L. Jimenez, R. Seila, J. A. de Gouw, B. de Foy, J. Fast, L. T. Molina, C. E. Kolb and D. R. Worsnop, Correlation of secondary organic aerosol with odd oxygen in Mexico City, *Geophys. Res. Lett.*, 2008, **35**, L15804.

115 L. I. Kleinman, S. R. Springston, P. H. Daum, Y.-N. Lee, L. J. Nunnermacker, G. I. Senum, J. Wang, J. Weinstein-Lloyd, M. L. Alexander, J. Hubbe, J. Ortega, M. R. Canagaratna and J. Jayne, The time evolution of aerosol composition over the Mexico City plateau, *Atmos. Chem. Phys.*, 2008, **8**, 1559–1575.

116 Q. J. Zhang, M. Beekmann, F. Drewnick, F. Freutel, J. Schneider, M. Crippa, A. S. H. Prevot, U. Baltensperger, L. Poulain, A. Wiedensohler, J. Sciare, V. Gros, A. Borbon, A. Colomb, V. Michoud, J. F. Doussin, H. A. C. Denier Van Der Gon, M. Haeffelin, J. C. Dupont, G. Siour, H. Petetin, B. Bessagnet, S. N. Pandis, A. Hodzic, O. Sanchez, C. Honoré and O. Perrussel, Formation of organic aerosol in the Paris region during the MEGAPOLI summer campaign: evaluation of the volatility-basis-set approach within the CHIMERE model, *Atmos. Chem. Phys.*, 2013, **13**, 5767–5790.

117 F. Rohrer, D. Brüning, E. S. Grobler, M. Weber, D. H. Ehhalt, R. Neubert, W. Schüßler and I. Levin, Mixing ratios and photostationary state of NO and NO_2 observed during the POPCORN field campaign at a rural site in Germany, *J. Atmos. Chem.*, 1998, **31**, 119–137.

118 J. P. Greenberg, A. B. Guenther, S. Madronich, W. Baugh, P. Ginoux, A. Druilhet, R. Delmas and C. Delon, Biogenic volatile organic compound emissions in central Africa during the Experiment for the Regional Sources and Sinks of Oxidants (EXPRESSO) biomass burning season, *J. Geophys. Res.: Atmos.*, 1999, **104**, 30659–30671.

119 K. Ashworth, S. Bucci, P. J. Gallimore, J. Lee, B. S. Nelson, A. Sanchez-Marroquín, M. B. Schimpf, P. D. Smith, W. S. Drysdale, J. R. Hopkins, J. D. Lee, J. R. Pitt, P. Di Carlo, R. Krejci and J. B. McQuaid, Megacity and local contributions to regional air pollution: an aircraft case study over London, *Atmos. Chem. Phys.*, 2020, **20**, 7193–7216.

120 R. Vautard, D. Martin, M. Beekmann, P. Drobinski, R. Friedrich, A. Jaubertie, D. Kley, M. Lattuati, P. Moral, B. Neinger and J. Theloke, Paris emission inventory diagnostics from ESQUIF airborne measurements and a chemistry transport model, *J. Geophys. Res.: Atmos.*, 2003, **108**, 1–21.

121 P. Zanis, P. Hadjinicolaou, A. Pozzer, E. Tyrlis, S. Dafka, N. Mihalopoulos and J. Lelieveld, Summertime free-tropospheric ozone pool over the eastern Mediterranean/Middle East, *Atmos. Chem. Phys.*, 2014, **14**, 115–132.

122 I. Coll, S. Pinceloup, P. E. Perros, G. Laverdet and G. Le Bras, 3D analysis of high ozone production rates observed during the ESCOMPTE campaign, *Atmos. Res.*, 2005, **74**, 477–505.

123 C. E. Reeves, P. Formenti, C. Afif, G. Ancellet, J. L. Attié, J. Bechara, A. Borbon, F. Cairo, H. Coe, S. Crumeyrolle, F. Fierli, C. Flamant, L. Gomes, T. Hamburger, C. Jambert, K. S. Law, C. Mari, R. L. Jones, A. Matsuki, M. I. Mead, J. Methven, G. P. Mills, A. Minikin, J. G. Murphy, J. K. Nielsen, D. E. Oram, D. J. Parker, A. Richter, H. Schlager, A. Schwarzenboeck and V. Thouret, Chemical and aerosol characterisation of the troposphere over West Africa during the monsoon period as part of AMMA, *Atmos. Chem. Phys.*, 2010, **10**, 7575–7601.

124 R. E. Shetter, D. H. Stedman and D. H. West, The $NO/NO_2/O_3$ photostationary state in Claremont, California, *J. Air Pollut. Control Assoc.*, 1983, **33**, 212–214.

125 Z. Y. W. Davis, S. Baray, C. A. McLinden, A. Khanbabakhani, W. Fujs, C. Csukat, J. Debosz and R. McLaren, Estimation of NO_x and SO_2 emissions from Sarnia, Ontario, using a mobile MAX-DOAS (Multi-Axis Differential Optical Absorption Spectroscopy) and a NO_x analyzer, *Atmos. Chem. Phys.*, 2019, **19**, 13871–13889.

126 R. Masiwal, C. Sharma, D. K. Shukla, D. Sethi, S. R. Radhakrishnan, R. K. Kotnala and B. C. Arya, Photochemistry of ozone over urban area: a case study for Delhi City, *Indian J. Phys.*, 2019, **93**, 415–425.

127 Z. H. Beygi, H. Fischer, H. D. Harder, M. Martinez, R. Sander, J. Williams, D. M. Brookes, P. S. Monks and J. Lelieveld, Oxidation photochemistry in the southern Atlantic boundary layer: unexpected deviations of photochemical steady state, *Atmos. Chem. Phys.*, 2011, **11**, 8497–8513.

128 T. A. Biesenthal, J. W. Bottenheim, P. B. Shepson, S.-M. Li and P. C. Brickell, The chemistry of biogenic hydrocarbons at a rural site in eastern Canada, *J. Geophys. Res.: Atmos.*, 1998, **103**, 25487–25498.

129 H. Singh and J. Kasting, Chlorine-hydrocarbon photochemistry in the marine troposphere and lower stratosphere, *J. Atmos. Chem.*, 1988, **7**, 261–285.

130 G. M. Handisides, C. Plass-Dülmer, S. Gilge, H. Bingemer and H. Berresheim, Hohenpeissenberg Photochemical Experiment (HOPE 2000): measurements and photostationary state calculations of OH and peroxy radicals, *Atmos. Chem. Phys.*, 2003, **3**, 1565–1588.

131 Y. Kanaya, Y. Sadanaga, K. Nakamura and H. Akimoto, Behavior of OH and HO_2 radicals during the Observations at a Remote Island of Okinawa (ORION99) field campaign 1. Observation using a laser-induced fluorescence instrument, *J. Geophys. Res.: Atmos.*, 2001, **106**, 24197–24208.

132 V. Michoud, A. Kukui, M. Camredon, A. Colomb, A. Borbon, K. Miet, B. Aumont, M. Beekmann, R. Durand-Jolibois, S. Perrier, P. Zapf, G. Siour, W. Ait-Helal, N. Locoge, S. Sauvage, C. Afif, V. Gros, M. Furger, G. Ancellet and J. F. Doussin, Radical budget analysis in a suburban European site during the MEGAPOLI summer field campaign, *Atmos. Chem. Phys.*, 2012, **12**, 11951–11974.

133 N. Carslaw, D. J. Creasey, D. E. Heard, A. C. Lewis, J. B. McQuaid, M. J. Pilling, P. S. Monks, B. J. Bandy and S. A. Penkett, Modeling OH, HO_2, and RO_2 radicals in the marine boundary layer: 1. Model construction and comparison with field measurements, *J. Geophys. Res.: Atmos.*, 1999, **104**, 30241–30255.

134 G. J. Frost, M. Trainer, G. Allwine, M. P. Buhr, J. G. Calvert, C. A. Cantrell, F. C. Fehsenfeld, P. D. Goldan, J. Herwehe, G. Hübler, W. C. Kuster, R. Martin, R. T. McMillen, S. A. Montzka, R. B. Norton, D. D. Parrish, B. A. Ridley, R. E. Shetter, J. G. Walega, B. A. Watkins, H. H. Westberg and E. J. Williams, Photochemical ozone production in the rural southeastern United States during the 1990 Rural Oxidants in the Southern Environment (ROSE) program, *J. Geophys. Res.: Atmos.*, 1998, **103**, 22491–22508.

135 L. I. Kleinman, P. H. Daum, D. G. Imre, J. H. Lee, Y. N. Lee, L. J. Nunnermacker, S. R. Springston, J. Weinstein-Lloyd and L. Newman, Ozone production in the New York City urban plume, *J. Geophys. Res.: Atmos.*, 2000, **105**, 14495–14511.

136 R. Imhoff, R. Valente, J. F. Meagher and M. Luria, The production of O_3 in an urban plume: airborne sampling of the Atlanta urban plume, *Atmos. Environ.*, 1995, **29**, 2349–2358.

137 M. Martinez, OH and HO_2 concentrations, sources, and loss rates during the Southern Oxidants Study in Nashville, Tennessee, Summer 1999, *J. Geophys. Res.*, 2003, **108**, 4617.

138 C. Spirig, A. Neftel, L. I. Kleinman and J. Hjorth, NO_x versus VOC limitation of O_3 production in the Po valley: local and integrated view based on observations, *J. Geophys. Res.*, 2002, **107**, 8191.

139 F. Gheusi, P. Durand, N. Verdier, F. Dulac, J.-L. Attié, P. Commun, B. Barret, C. Basdevant, A. Clenet, S. Derrien, A. Doerenbecher, L. El Amraoui, A. Fontaine, E. Hache, C. Jambert, E. Jaumouillé, Y. Meyerfeld, L. Roblou and F. Tocquer, Adapted ECC ozonesonde for long-duration flights aboard boundary-layer pressurised balloons, *Atmos. Meas. Tech.*, 2016, **9**, 5811–5832.

140 M. Beekmann and R. Vautard, A modelling study of photochemical regimes over Europe: robustness and variability, *Atmos. Chem. Phys.*, 2010, **10**, 10067–10084.

141 S. Sillman, The use of NO_y, H_2O_2, and HNO_3 as indicators for ozone-NO_x-hydrocarbon sensitivity in urban locations, *J. Geophys. Res.*, 1995, **100**, 14175.

142 S. Sillman, O_3-NO_x-VOC sensitivity and NO_x-VOC indicators in Paris: results from models and atmospheric pollution over the Paris area (ESQUIF) measurements, *J. Geophys. Res.*, 2003, **108**, 8563.

143 T. B. Ryerson, M. P. Buhr, G. J. Frost, P. D. Goldan, J. S. Holloway, G. Hübler, B. T. Jobson, W. C. Kuster, S. A. McKeen, D. D. Parrish, J. M. Roberts, D. T. Sueper, M. Trainer, J. Williams and F. C. Fehsenfeld, Emissions lifetimes and ozone formation in power plant plumes, *J. Geophys. Res.: Atmos.*, 1998, **103**, 22569–22583.

144 L. R. F. Henneman, H. Shen, C. Liu, Y. Hu, J. A. Mulholland and A. G. Russell, Responses in Ozone and Its Production Efficiency Attributable to Recent and Future Emissions Changes in the Eastern United States, *Environ. Sci. Technol.*, 2017, **51**, 13797–13805.

145 L. J. Nunnermacker, D. Imre, P. H. Daum, L. Kleinman, Y.-N. Lee, J. H. Lee, S. R. Springston, L. Newman, J. Weinstein-Lloyd, W. T. Luke, R. Banta, R. Alvarez, C. Senff, S. Sillman, M. Holdren, G. W. Keigley and X. Zhou, Characterization of the Nashville urban plume on July 3 and July 18, 1995, *J. Geophys. Res.: Atmos.*, 1998, **103**, 28129–28148.

146 I. B. Pollack, T. B. Ryerson, M. Trainer, D. D. Parrish, A. E. Andrews, E. L. Atlas, D. R. Blake, S. S. Brown, R. Commane, B. C. Daube, J. A. de Gouw, W. P. Dubé,

J. Flynn, G. J. Frost, J. B. Gilman, N. Grossberg, J. S. Holloway, J. Kofler, E. A. Kort, W. C. Kuster, P. M. Lang, B. Lefer, R. A. Lueb, J. a. Neuman, J. B. Nowak, P. C. Novelli, J. Peischl, a. E. Perring, J. M. Roberts, G. Santoni, J. P. Schwarz, J. R. Spackman, N. L. Wagner, C. Warneke, R. A. Washenfelder, S. C. Wofsy and B. Xiang, Airborne and ground-based observations of a weekend effect in ozone, precursors, and oxidation products in the California South Coast Air Basin, *J. Geophys. Res.: Atmos.*, 2012, **117**(3), DOI: **10.1029/2011JD016772**.

147 C. C. K. Chou, C.-Y. Tsai, C.-J. Shiu, S. C. Liu and T. Zhu, Measurement of NO_y during Campaign of Air Quality Research in Beijing 2006 (CAREBeijing-2006): implications for the ozone production efficiency of NO_x, *J. Geophys. Res.*, 2009, **114**, D00G01.

148 C. C.-K. Chou, C.-Y. Tsai, C.-C. Chang, P.-H. Lin, S. C. Liu and T. Zh, Photochemical production of ozone in Beijing during the 2008 Olympic Games, *Atmos. Chem. Phys. Discuss.*, 2011, **11**, 16553–16584.

149 B. Z. Ge, X. B. Xu, W. L. Lin, J. Li and Z. F. Wang, Impact of the regional transport of urban Beijing pollutants on downwind areas in summer: ozone production efficiency analysis, *Tellus B*, 2012, **64**, 17348.

150 M. Ninneman, K. L. Demerjian and J. J. Schwab, Ozone Production Efficiencies at Rural New York State Locations: Relationship to Oxides of Nitrogen Concentrations, *J. Geophys. Res.: Atmos.*, 2019, **124**, 2363–2376.

151 M. Trainer, D. D. Parrish, P. D. Goldan, J. Roberts and F. C. Fehsenfeld, Review of observation-based analysis of the regional factors influencing ozone concentrations, *Atmos. Environ.*, 2000, **34**, 2045–2061.

152 C. Granier, S. Darras, H. Denier Van Der Gon, D. Jana, N. Elguindi, G. Bo, G. Michael, G. Marc, J.-P. Jalkanen and J. Kuenen, *The Copernicus Atmosphere Monitoring Service Global and Regional Emissions*, April 2019 version, 2019.

153 S. Tran, B. Bonsang, V. Gros, I. Peeken, R. Sarda-Esteve, A. Bernhardt and S. Belviso, A survey of carbon monoxide and non-methane hydrocarbons in the Arctic Ocean during summer 2010, *Biogeoscience*, 2013, **10**(3), 1909–1935, DOI: **10.5194/bg-10-1909-2013**.

154 V. Gros, K. Tsigaridis, B. Bonsang, M. Kanakidou and C. Pio, Factors controlling the diurnal variation of CO above a forested area in southeast Europe, *Atmos. Environ.*, 2002, **36**(19), 3127–3135, DOI: **10.1016/S1352-2310(02)00237-6**.

155 H. M. Worden, A. A. Bloom, J. R. Worden, Z. Jiang, E. A. Marais, T. Stavrakou, B. Gaubert and F. Lacey, New constraints on biogenic emissions using satellite-based estimates of carbon monoxide fluxes, *Atmos. Chem. Phys.*, 2019, **19**, 13569–13579.

156 J. Cuesta, Y. Kanaya, M. Takigawa, G. Dufour, M. Eremenko, G. Foret, K. Miyazaki and M. Beekmann, Transboundary ozone pollution across East Asia: daily evolution and photochemical production analysed by IASI+GOME2 multispectral satellite observations and model, *Atmos. Chem. Phys.*, 2018, **18**, 9499–9525, **https://doi.org/10.5194/acp-18-9499-2018**.